nature medicine

DKK2 imparts tumor immunity evasion through β-catenin-independent suppression of cytotoxic immune-cell activation

Qian Xiao[1,10], Jibo Wu[2,10], Wei-Jia Wang[1,10], Shiyang Chen[3], Yingxia Zheng[1], Xiaoqing Yu[4], Katrina Meeth[5], Mahnaz Sahraei[1], Alfred L M Bothwell[6,7], Lieping Chen[6,7], Marcus Bosenberg[5,7], Jianfeng Chen[3], Veronika Sexl[8], Le Sun[9], Lin Li[2], Wenwen Tang[1] & Dianqing Wu[1,6]

Immunotherapy offers new options for cancer treatment, but efficacy varies across cancer types. Colorectal cancers (CRCs) are largely refractory to immune-checkpoint blockade, which suggests the presence of yet uncharacterized immune-suppressive mechanisms. Here we report that the loss of adenomatosis polyposis coli (APC) in intestinal tumor cells or of the tumor suppressor PTEN in melanoma cells upregulates the expression of Dickkopf-related protein 2 (DKK2), which, together with its receptor LRP5, provides an unconventional mechanism for tumor immune evasion. DKK2 secreted by tumor cells acts on cytotoxic lymphocytes, inhibiting STAT5 signaling by impeding STAT5 nuclear localization via LRP5, but independently of LRP6 and the Wnt–β-catenin pathway. Genetic or antibody-mediated ablation of DKK2 activates natural killer (NK) cells and CD8$^+$ T cells in tumors, impedes tumor progression, and enhances the effects of PD-1 blockade. Thus, we have identified a previously unknown tumor immune-suppressive mechanism and immunotherapeutic targets particularly relevant for CRCs and a subset of melanomas.

Significant advances, particularly in immunotherapy, have been made in the treatment of cancers, a leading cause of death in humans[1–6]. Immune-checkpoint inhibitors, including anti-PD1 and anti-CTLA4, have shown clinical efficacy for some tumors, but not for many others, including CRCs[5,7–9]. Although mechanisms for resistance and/or insensitivity to current checkpoint inhibitors have been described[10], there are more mechanisms for tumor immune modulation yet to be discovered.

NK cells and CD8$^+$ T lymphocytes are the cytotoxic effector immune cells that are capable of directly killing tumor cells. The cytotoxic activity of NK cells and CD8$^+$ T cells is regulated by complex mechanisms, including those involving cytokines. IL-15 is a key cytokine that controls all aspects of NK cell biology[11] and is also important for the development and function of CD8$^+$ intestinal intraepithelial lymphocytes (IELs)[11–14]. In addition, it regulates effector and memory CD8$^+$ T cell development and function and confers T cell resistance to regulatory T cells (T_{reg} cells)[11,12,15,16]. IL-15 signals through its receptor, which consists of an IL-15Rα chain, an IL-2/IL-15Rβ chain, and a common cytokine-receptor γ-chain. IL-15 induces phosphorylation of STAT5 via JAK1 and JAK3. Phosphorylated STAT5 (pSTAT5) accumulates in the nucleus to regulate gene transcription. IL-15 also activates the PI3K–AKT, mTOR, and MAPK pathways. IL-15 stimulates cytotoxic effector functions by increasing the production of perforin and granzyme B (GZMB) through these pathways[11,12,17,18].

Wnt-signaling pathways control a wide range of cellular processes[19–22]. The Wnt–β-catenin pathway is initiated by two types of cell-surface receptors: low-density lipoprotein receptor-related proteins 5 and 6 (LRP5 and LRP6, respectively), and Frizzled proteins[23]. Dysregulation of Wnt–β-catenin signaling is associated with many human diseases, including cancer[19–22]. Hyperactivation of the Wnt–β-catenin pathway can lead to aberrant cell growth and tumor formation. More than 80% of CRCs harbor loss-of-function mutations in the gene encoding APC, a suppressor of the Wnt–β-catenin pathway[24].

DKK2 (refs. 21,25) inhibits Wnt–β-catenin signaling by binding to LRP5 and LRP6 (ref. 26). DKK2 has a less critical role in vertebrate development[27–29] and adult life. DKK2 deficiency leads to decreased blood glucose[30] and a moderate reduction in bone mass[28]. As DKK2

[1]Vascular Biology and Therapeutic Program and Department of Pharmacology, Yale School of Medicine, New Haven, Connecticut, USA. [2]State Key Laboratory of Molecular Biology, CAS Center for Excellence in Molecular Cell Science, Innovation Center for Cell Signaling Network, Institute of Biochemistry and Cell Biology, Shanghai Institutes for Biological Sciences, Chinese Academy of Sciences, University of Chinese Academy of Sciences, Shanghai, China. [3]State Key Laboratory of Cell Biology, CAS Center for Excellence in Molecular Cell Science, Shanghai Institute of Biochemistry and Cell Biology, Chinese Academy of Sciences, University of Chinese Academy of Sciences, Shanghai, China. [4]Biostatistics Department, Yale University, New Haven, Connecticut, USA. [5]Departments of Dermatology and Pathology, Yale School of Medicine, New Haven, Connecticut, USA. [6]Department of Immunobiology, Yale School of Medicine, New Haven, Connecticut, USA. [7]Yale Cancer Center, Yale School of Medicine, New Haven, Connecticut, USA. [8]Institute of Pharmacology and Toxicology, Department for Biomedical Sciences, University of Veterinary Medicine Vienna, Vienna, Austria. [9]AbMax, Beijing, China. [10]These authors contributed equally to this work. Correspondence should be addressed to D.W. (dan.wu@yale.edu), W.T. (Wenwen.tang@yale.edu) or L.L. (lin.li@sibs.ac.cn).

Received 7 March 2017; accepted 12 January 2018; published online 12 February 2018; doi:10.1038/nm.4496

is a Wnt antagonist[27,28,31–33], the conventional wisdom is that DKK2 inactivation might increase Wnt activity and lead to or accelerate cancer formation. However, our findings in this study were contrary to what was expected: DKK2, which shows upregulated expression in human CRCs and cells with APC-loss mutations, promoted tumor progression by suppressing the activation of immune effector cells.

RESULTS

Loss of APC drives DKK2 expression

Analysis of the Gaedcke cohort[34] in the Oncomine database (https://www.oncomine.org) showed that DKK2 expression is significantly upregulated in human CRC samples compared with its expression in non-tumorous colorectal tissues ($P < 0.01$; **Supplementary Fig. 1a**), which is in agreement with a previous finding[35]. Analysis of Cancer Genome Atlas Network data sets[36] further revealed that DKK2 expression in microsatellite-stable (MSS) CRCs, more than 80% of which harbor *APC* mutations, is significantly higher than that in microsatellite-instable CRCs ($P < 0.05$; **Supplementary Fig. 1a**). In mice, the *Dkk2* mRNA content in the intestinal polyps of $Apc^{Min/+}$ mice, a mouse genetic intestinal tumor model[37], was about four times higher than that in normal intestinal tissue (**Supplementary Fig. 1b**). Immunostaining of DKK2 protein and *in situ* hybridization of *Dkk2* mRNA confirmed upregulated DKK2 expression in the polyps (**Supplementary Fig. 1c,d**). In mouse colon cancer MC38 cells in which *Apc* was mutated by CRISPR–Cas9, DKK2 expression was markedly upregulated in APC-null cells (**Supplementary Fig. 1e**). This upregulation was suppressed by β-catenin small interfering RNAs (**Supplementary Fig. 1f**), which suggested the involvement of β-catenin in driving DKK2 expression. APC loss also led to upregulation of DKK2 expression in human colon cancer HCT116 cells (**Supplementary Fig. 1g**). Therefore, we conclude that APC loss drives DKK2 expression in both mouse and human CRC cells.

DKK2 blockade suppresses APC-loss-induced tumor formation

Analysis of the TCGA CRC data sets showed that high DKK2 expression correlates with poor survival rates (**Supplementary Fig. 1h**). This suggests that DKK2 may have an important role in CRCs. Concordantly, DKK2 deficiency was associated with significantly reduced intestinal polyp burdens in both male and female $Apc^{Min/+}$ mice compared with those in wild-type mice (**Fig. 1a–c** and

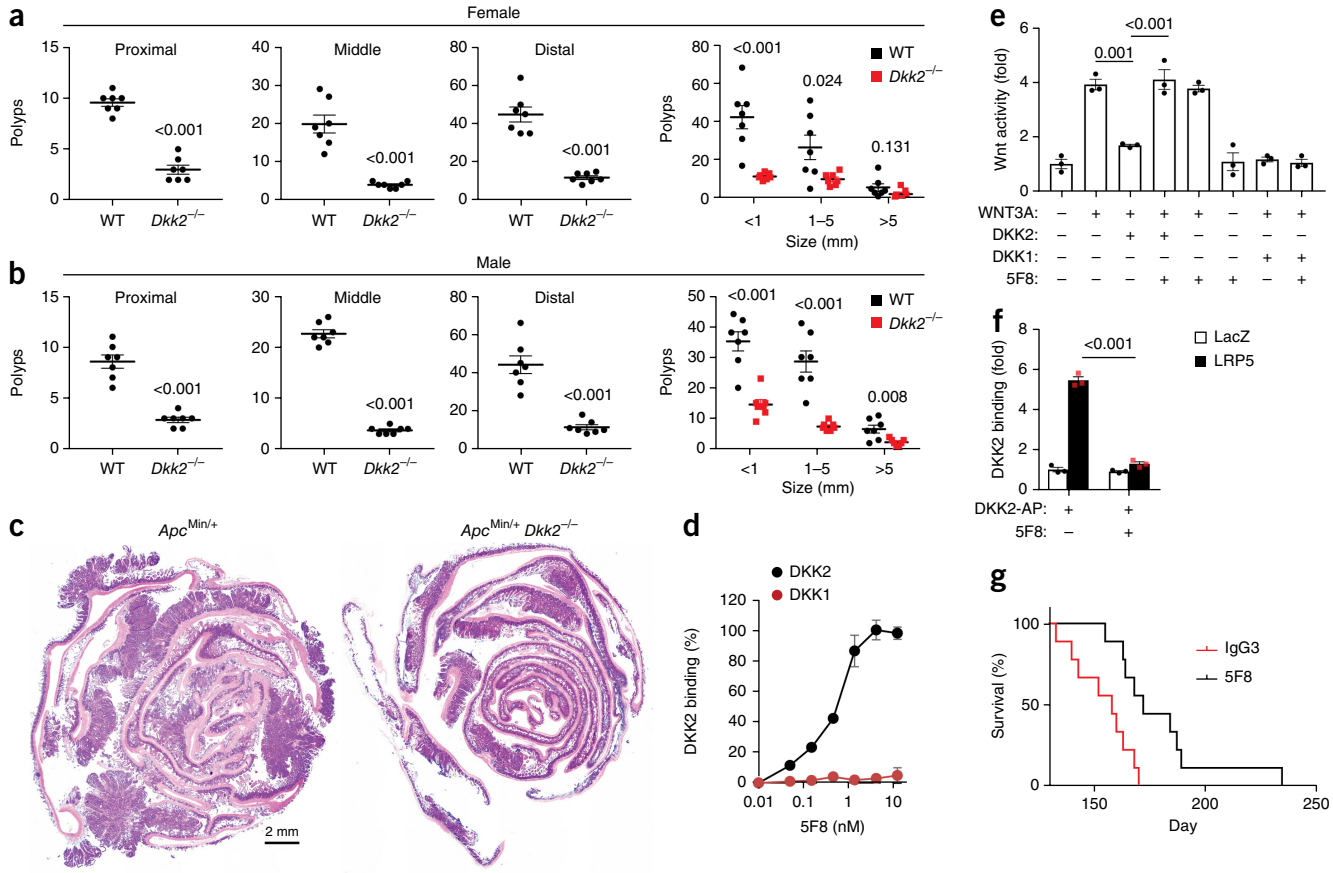

Figure 1 DKK2 blockade reduces tumor burdens in $Apc^{Min/+}$ mice. (**a**–**c**) Littermates of $Apc^{Min/+}$ and $Apc^{Min/+}Dkk2^{-/-}$ mice were housed for 20 weeks (female; **a**) or 22 weeks (male; **b**), and polyps in proximal, middle, and distal intestine were counted and measured under a stereomicroscope after staining with methylene blue (two-tailed Student's *t*-test for polyp number; two-way ANOVA for size; $n = 7$). Representative H&E staining images of intestinal sections from an $Apc^{Min/+}$ mouse and its $Apc^{Min/+}Dkk2^{-/-}$ littermate are shown (**c**). Single data points represent individual mice. WT, wild-type. (**d**) Binding of anti-DKK2 antibody 5F8 to mouse DKK2 and DKK1 proteins as shown by ELISA ($n = 3$). (**e**) HEK293 cells were transfected with the Wnt reporter gene plasmid TOPFlash and treated with WNT3A conditioned medium (CM), DKK2 CM or DKK1 CM, and 5F8 (18 μg/ml) as indicated (one-way ANOVA; $n = 3$). (**f**) HEK293 cells were transfected with LacZ (control) or LRP5 expression plasmid. The plot shows the binding of DKK2-AP fusion protein to cells in the presence or absence of 5F8 (18 μg/ml) (two-way ANOVA; $n = 3$). (**g**) Mice (16-week-old males) were treated with 5F8 or an isotype antibody (IgG3) (8 mg/kg i.p. once per week) and their survival was recorded ($P = 0.004$; two-sided Mantel–Cox log-rank test; $n = 9$). Data are presented as mean ± s.e.m. (**a**,**b**) or mean ± s.d. (**d**–**f**), with *P* values shown within plots where relevant; experiments in **d**–**f** were repeated twice, and those in **a**–**c** were done once.

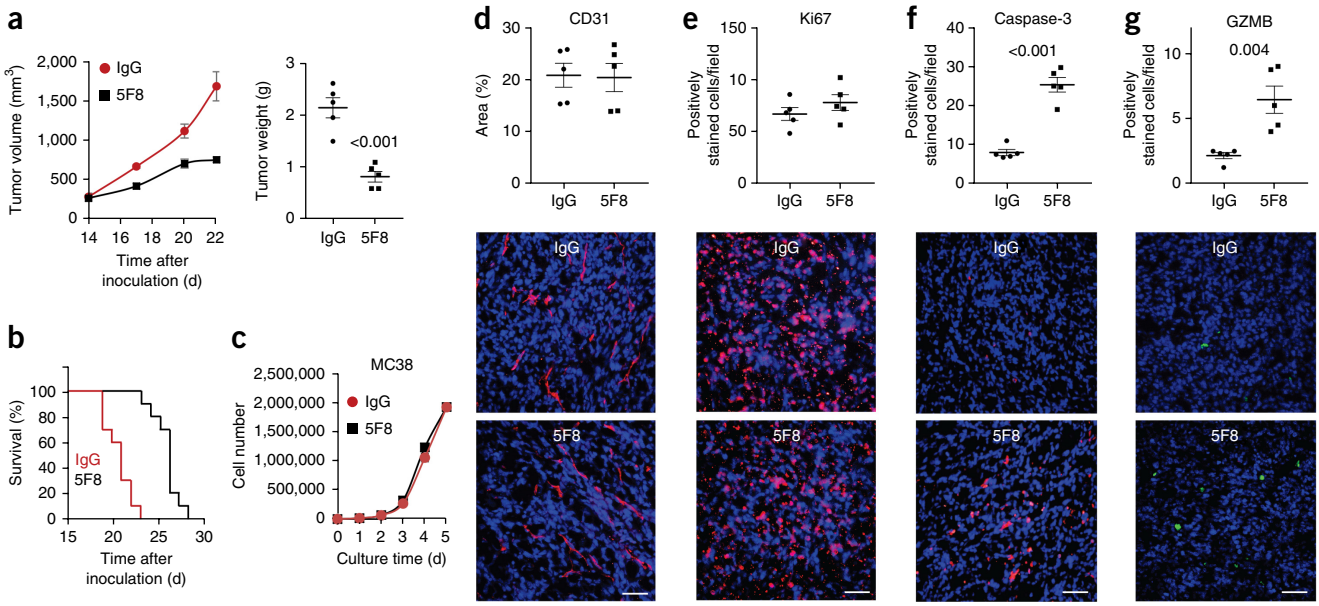

Figure 2 DKK2 blockade impedes tumor progression in the MC38 syngeneic tumor model. (**a**,**b**) C57BL/6 mice inoculated with MC38 cells were treated with 5F8 (10 mg/kg i.p. every 3 d) starting at day 14 after inoculation. Tumors from some of the mice were collected at day 22 and weighed ($P = 0.002$ and $P < 0.001$ for tumor growth at days 20 and 22, respectively; two-way ANOVA; two-tailed Student's *t*-test for tumor weight; $n = 5$). The rest of the mice were used for evaluation of survival ($P = 0.004$ for 5F8-treated versus IgG-treated; two-sided log-rank Mantel–Cox test; $n = 10$). (**c**) The 5F8 antibody did not affect MC38 cell growth in culture ($n = 4$). (**d**–**g**) Effects of 5F8 treatment on tumor angiogenesis, tumor cell proliferation and apoptosis, and numbers of GZMB$^+$ cells were evaluated by staining of the sections of tumor collected in **a** for CD31 (**d**), Ki67 (**e**), cleaved caspase-3 (**f**), and GZMB (**g**). The sections were also counterstained with DAPI. Five independent sections per tumor and five tumors per group were examined (two-sided Student's *t*-test). Data are presented as mean ± s.e.m., with *P* values shown in plots where relevant (**a**,**c**–**g**). Individual data points represent individual tumors. All experiments were repeated twice. Scale bars, 100 μm.

Supplementary Fig. 1i). We then generated a mouse monoclonal antibody to DKK2 (designated as 5F8), and found that it bound to mouse DKK2, but not to DKK1 (**Fig. 1d**). The antibody inhibited DKK2-mediated, but not DKK1-mediated, antagonism of Wnt activation (**Fig. 1e**). Moreover, 5F8 blocked the binding of DKK2 to LRP5 (**Fig. 1f**). Administration of 5F8 significantly extended survival and reduced intestinal polyp burdens (depending on the presence of DKK2) in $Apc^{Min/+}$ mice compared with mice treated with an isotype control antibody (**Fig. 1g** and **Supplementary Fig. 2a–c**). Of note, an antibody to PD-1 showed no significant effect on polyp burden in these mice (data not shown), which is consistent with the reported lack of therapeutic efficacy of PD-1 blockade on human MSS CRCs[5,7–9]. These results together support the conclusion that DKK2 blockade suppresses the formation of intestinal polyps, a form of non-malignant tumor, caused by APC loss. Thus, rather than impeding it, as one might have predicted on the basis of the known mechanism of action, DKK2 supports tumor progression.

DKK2 blockade modulates tumor immune microenvironment

In experiments with a syngeneic mouse colon cancer model, 5F8 significantly inhibited the growth of subcutaneously grafted MC38 cells in C57BL/6 mice (**Fig. 2a**) and extended the survival of tumor-bearing mice (**Fig. 2b**) compared with that in mice treated with isotype control antibody (IgG3). As 5F8 did not affect the growth of MC38 cells in culture (**Fig. 2c**), the antibody might impede tumor progression by altering the tumor microenvironment. Immunohistological examination of the MC38 tumors revealed that 5F8 had no significant effects on angiogenesis (**Fig. 2d**) or tumor cell proliferation (**Fig. 2e**). However, treatment with 5F8 increased the number of apoptotic cells (**Fig. 2f**) and GZMB$^+$ cells (**Fig. 2g**). We also observed increases in apoptosis and GZMB expression in $Apc^{Min/+}Dkk2^{-/-}$ polyps compared with that in $Apc^{Min/+}$ polyps (**Supplementary Fig. 2d**,**e**) and in 5F8-treated polyps compared with that in IgG3-treated polyps (data not shown). DKK2 blockade did not significantly affect proliferation, infiltration of cytotoxic immune cells, or differentiation in the polyps (**Supplementary Fig. 2f–i**). Because GZMB is largely produced by NK cells and CD8$^+$ T cells and induces tumor cell apoptosis[38], the above results suggest that DKK2 blockade may modulate the immune microenvironment. In support of this conclusion, when we grafted MC38 cells onto immunodeficient NSG mice, which lack mature leukocytes, and administered 5F8, the antibody did not show any tumor-suppressive effect (**Fig. 3a**,**b**).

DKK2 blockade enhances NK cell and CD8$^+$ T cell activation

Consistent with the immunostaining results (**Fig. 2g**), flow cytometry analysis of tumor-infiltrating leukocytes showed that 5F8 treatment increased the amount of GZMB in both CD8$^+$ T cells and NK1.1$^+$ T cells (**Supplementary Fig. 3a–g**). In contrast, there were no differences between 5F8-treated and isotype-treated samples in terms of the percentages of myeloid cells (Gr1^{hi}CD11b^{hi} or Gr1^{lo}CD11b^{hi}), CD4$^+$ T cells, CD8$^+$ T cells, T_{reg} cells (CD4$^+$CD25$^+$Foxp3$^+$), and NK1.1$^+$ T cells (**Supplementary Fig. 3b–e**). Analysis of leukocytes in tumor-draining lymph nodes showed that there were no differences among the populations of CD4$^+$ T cells, CD8$^+$ T cells, or NK1.1$^+$ T cells (**Supplementary Fig. 3h**,**i**), whereas there was a trend for increased amounts of GZMB in CD8$^+$ T cells (**Supplementary Fig. 3j**) and a substantial increase in GZMB expression in NK1.1$^+$ T cells in 5F8-treated samples compared with that in IgG3-treated samples (**Supplementary Fig. 3k**). We also observed increased numbers of GZMB$^+$CD8$^+$ T cells in Peyer's patches and draining lymph

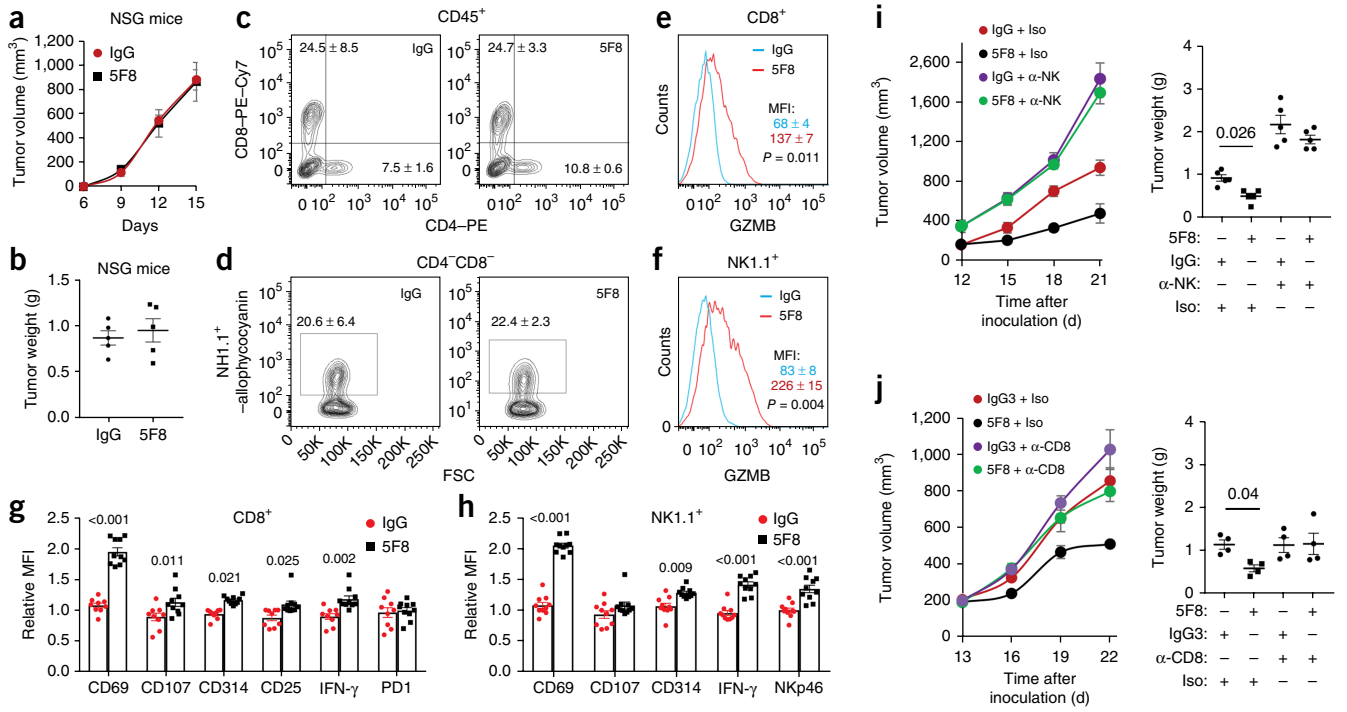

Figure 3 DKK2 blockade enhances cytotoxic immune cell activation. (**a**,**b**) MC38 cells were injected subcutaneously into NSG mice ($n = 5$), and treatment (10 mg/kg every 3 d) commenced at day 6 after injection The plots show changes in tumor volume over time (**a**) and tumor weight (**b**) in 5F8-treated versus control mice. (**c**–**h**) MC38 cells were injected subcutaneously into C57BL/6 mice. When tumors reached 600 mm^3 on average, the mice were given one injection of antibody (10 mg/kg i.p.). Tumors were collected 24 h later for flow cytometry analysis (two-tailed Student's *t*-test; $n = 10$). Panel **c** is pre-gated for CD45, and panels **d**, **e**, and **g** are derived from panel **c**. Panels **f** and **h** are derived from panel **d**. Cell numbers: 4,192 ± 446 (IgG-treated) and 4,431 ± 357 (5F8-treated) $CD8^+$ T cells per 10^6 tumor cells; 3,600 ± 501 (IgG-treated) and 3,200 ± 329 (5F8-treated) $NK1.1^+$ cells per 10^6 tumor cells (mean ± s.e.m.). MFI, mean fluorescence intensity; PE, phycoerythrin. (**i**,**j**) C57BL/6 mice were inoculated subcutaneously with MC38 cells. Treatment with 5F8 (10 mg/kg i.p. every 3 d) commenced at day 12 after inoculation for the NK cell–depletion experiment or at day 13 after inoculation for the $CD8^+$ T cell–depletion experiment (*P* values for tumor growth: 0.008 for **i** and 0.003 for **j**, IgG + isotype control antibody (Iso) versus 5F8 + Iso). Tumor weight *P* values are shown in plots; $n = 5$; two-way ANOVA. All data are presented as mean ± s.e.m. Experiments were repeated three times (**a**–**h**) or were done once (**i**–**j**).

nodes for intestinal tumors in *Dkk2*$^{-/-}$*Apc*$^{Min/+}$ mice compared with those in *Apc*$^{Min/+}$ mice, whereas there were no significant differences in the $CD4^+$ and $CD8^+$ T cell populations between these mouse groups (**Supplementary Fig. 4a**,**b**).

To exclude the effect of tumor size on the flow cytometry results, we treated MC38-tumor-bearing mice with antibodies for only 24 h before analysis. At this time point, there were no obvious differences in tumor size. Although there were still no significant differences in the populations of $CD4^+$ T cells, $CD8^+$ T cells, or $NK1.1^+$ T cells (**Fig. 3c**,**d**), we observed strong increases in GZMB expression in tumor-infiltrating $CD8^+$ T cells and $NK1.1^+$ T cells in 5F8-treated mice compared with that in isotype-treated mice (**Fig. 3e**,**f**). We also observed significant increases in levels of other activation markers of $CD8^+$ T cells and NK cells, including CD69, CD107a, CD314, IFN-γ, and CD25 on $CD8^+$ T cells, and CD69, IFN-γ, NKp46, and CD314 on NK cells (**Fig. 3g**,**h**). We did not observe any significant changes in levels of Ki67, T-bet, Eomes, phospho-mTOR, phospho-S6K, phospho-AKT, KLGR1, CD122, or CD127 in 5F8-treated $CD8^+$ T cells or $NK1.1^+$ cells compared with levels in cells from isotype-treated mice (**Supplementary Fig. 4c**,**d**). Acute 5F8 treatment also considerably increased the number of $GZMB^+CD8^+$ T cells in Peyer's patches of *Apc*$^{Min/+}$ mice compared with those in IgG-treated mice, without affecting the overall size of the T cell populations (**Supplementary Fig. 4e**,**f**).

To assess the importance of cytotoxic immune effector cells in DKK2-blockade-mediated tumor suppression, we depleted NK cells with anti-NK1.1 and depleted $CD8^+$ T cells with anti-CD8 in the MC38 tumor model (**Supplementary Fig. 5a**–**c**). Depletion of either NK cells or $CD8^+$ T cells largely diminished the tumor-suppressive effect of 5F8, with NK cell depletion perhaps having a stronger effect (**Fig. 3i**,**j**). We also depleted these same cell populations in the *Apc*$^{Min/+}$ model. Whereas $NK1.1^+$ T cell depletion did not noticeably alter the effect of 5F8 on polyp formation, $CD8^+$ T cell depletion largely abrogated the effect of 5F8 (**Supplementary Fig. 5d**). These results indicate that cytotoxic immune effector cells have important roles in DKK2-blockade-mediated suppression of tumor formation.

DKK2 directly suppresses cytotoxic immune cells

Next we assessed the effect of DKK2 blockade on the cytotoxicity of primary NK cells. Inclusion of 5F8 caused a marked increase in GZMB expression in NK cells (**Fig. 4a**) and decreased tumor cell viability (**Fig. 4b**) in cocultures of IL-15-expanded primary mouse NK cells and MC38 cells. By contrast, in cultures of only one or the other cell type, 5F8 treatment showed little effect on GZMB expression in NK cells (**Fig. 4c**) or on the viability of MC38 cells (**Fig. 2c**).

We carried out microarray gene expression analyses, and did not observe significantly altered expression of IL-2, IL-15, MHC-I haplotypes, NKG2D ligands (RAE-1α-ε, MULT-1, and H60a-c), Fas, or TRAILR1/2, all of which are important for NK cell activity, in 5F8-treated MC38 cells or tumors compared with expression in IgG3-treated samples (data not shown). In addition, *Dkk2* mRNA

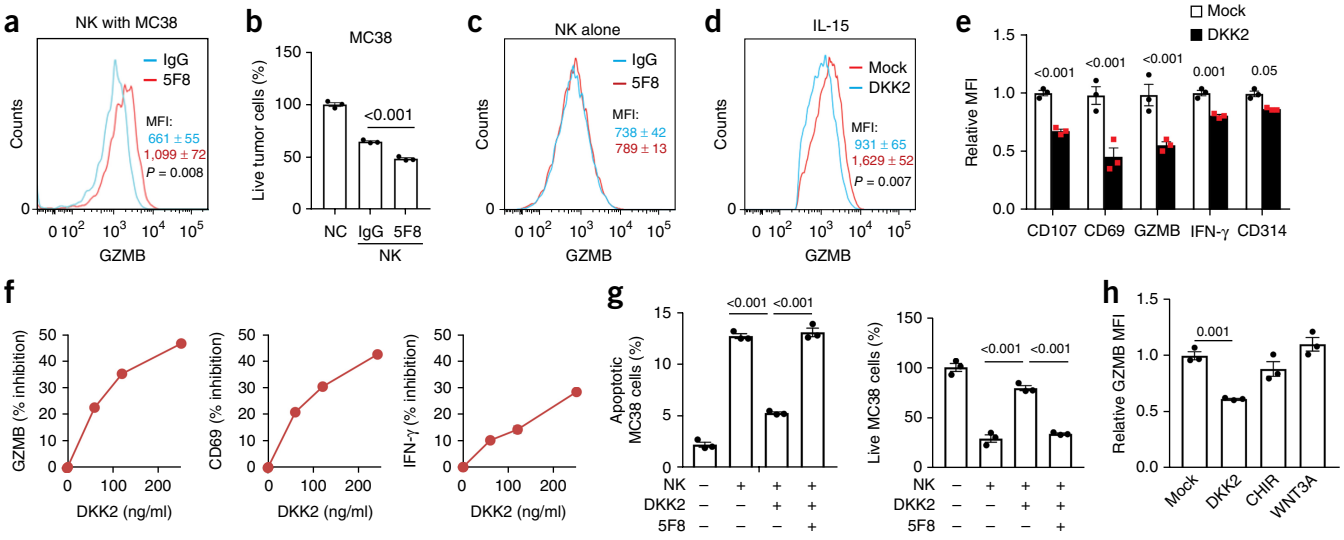

Figure 4 DKK2 directly suppresses NK cell activation. (**a**–**c**) Primary mouse NK cells expanded with IL-15 were added to MC38 cells that had been seeded 1 d prior in the presence of 5F8 or IgG3 (36 μg/ml) for 9 h. GZMB expression in NK cells was examined by flow cytometry (**a**,**c**; two-tailed Student's *t*-test; $n = 4$), whereas the number of live tumor cells was determined by a Guava cell cytometer (**b**; one-way ANOVA; $n = 4$). (**d**–**f**) Isolated primary mouse NK cells were cultured with IL-15 (50 ng/ml) for 24 h. DKK2 protein (400 ng/ml for **d** and **e**; varying amounts for **f**) was then added for another 24 h, after which the samples were analyzed by flow cytometry (*P* values for DKK2 versus mock; $n = 3$; two-sided Student's *t*-test). (**g**) Primary NK cells were expanded in IL-15 (50 ng/ml) for 24 h and then treated with or without DKK2 (400 ng/ml) or 5F8 (36 μg/ml) for 24 h. The NK cells were then added at a 7:1 ratio to MC38 cells that had been seeded the day before. The number of apoptotic MC38 cells was determined after 6 h, and the number of live MC38 cells was determined after 9 h of coculture ($n = 3$; one-way ANOVA). (**h**) Isolated primary mouse NK cells were cultured with IL-15 (50 ng/ml) for 24 h. DKK2 protein (400 ng/ml), WNT3A (100 ng/ml), and GSK3 inhibitor CHIR99021 (CHIR; 1 μM) were then added for another 24 h, after which the samples were analyzed by flow cytometry ($n = 3$; one-way ANOVA). Data are presented as mean ± s.e.m. (**a**–**e**,**g**,**h**) with *P* values shown in plots where relevant (**a**,**b**,**d**,**e**,**g**,**h**), and the experiments were repeated three (**a**–**f**) or two (**g**,**h**) times; data in **f** are representative of one of the three repeated experiments.

was hardly detectable by RT-PCR in NK cells, whereas it was readily detectable in MC38 cells (**Supplementary Fig. 1e**). On the basis of both these results and the aforementioned coculture results, we postulated that tumor-cell-produced DKK2 might act directly on NK cells. Indeed, the addition of recombinant DKK2 protein to primary NK cells cultured with IL-15 caused 5F8-reversible reductions in levels of GZMB, CD69, IFN-γ, CD107a, CD314 (**Fig. 4d**,**e**), KLRG1, and CD122 (**Supplementary Fig. 6a**). These inhibitory effects of DKK2 were dose dependent (**Fig. 4f**) and were also observed for NK cells stimulated with IL-12 and IL-18 (**Supplementary Fig. 6b**). DKK2 also had significant effects on tumor-killing ability, as NK cells pretreated with DKK2 had a reduced ability to cause tumor cell apoptosis and death (**Fig. 4g**). Additionally, DKK2 inhibited IL-15-mediated activation of human NK cells and $CD8^+$ T cells isolated from peripheral blood (**Supplementary Fig. 6c**,**d**). Furthermore, DKK2 suppressed the response to IL-15 in mouse primary $CD8^+$ T cells isolated from spleen and $CD8^+$ IELs (**Supplementary Fig. 6d**,**e**). Thus, DKK2 could directly suppress the activation of both human and mouse immune effector cells.

DKK2 inhibits NK cell activation independently of Wnt–β-catenin signaling

Next, we tested whether Wnt–β-catenin signaling is responsible for NK cell regulation by DKK2, as DKK2 can inhibit this pathway. WNT3A induced a strong increase in Wnt reporter gene activity, which could be inhibited by DKK2 (**Supplementary Fig. 7a**). WNT3A also induced β-catenin accumulation in primary NK cells (**Supplementary Fig. 7b**). However, WNT3A did not alter GZMB expression in NK cells (**Fig. 4h**). Concordantly, the GSK3 inhibitor CHIR99021, which increases β-catenin stability by bypassing Wnt and its receptors and strongly stimulated Wnt reporter gene activity (**Supplementary Fig. 7a**), did not affect primary NK cells (**Fig. 4h**). Therefore, it seems likely that DKK2-mediated inhibition of NK cell activation is independent of Wnt–β-catenin signaling. These results also distinguish the mechanism of action of DKK2 from that described in recent reports indicating involvement of Wnt–β-catenin signaling in the modulation of tumor immune microenvironments[39,40].

DKK2 impedes nuclear localization of phosphorylated STAT5

Given that DKK2 suppressed cytotoxic immune cell activation by IL-15, we examined the effects of DKK2 treatment on various signaling events stimulated by IL-15. Although we observed reductions in amounts of GZMB and perforin proteins in DKK2-treated samples, we did not detect any notable changes in the phosphorylation of STAT5, ERK, AKT (**Fig. 5a**), MTOR, S6K, STAT1, or STAT4 (**Supplementary Fig. 8a**,**b**). DKK2 treatment did not induce any changes in cell size (**Supplementary Fig. 8c**), and it is known that DKK2 does not alter the MTORC1 pathway, which can affect GZMB expression in NK cells[17,18]. However, RNA-seq analysis of DKK2-treated and mock-treated primary NK cells suggested an alteration in STAT5 signaling after DKK2 treatment (**Supplementary Fig. 8d**,**e** and **Supplementary Table 1**). We thus examined the localization of pSTAT5 a step downstream of STAT5 phosphorylation. Whereas IL-15 induced nuclear localization of pSTAT5 as expected, cytosolic localization of pSTAT5 was readily detected in DKK2-treated cells (**Fig. 5b** and **Supplementary Fig. 8f**). This result was further confirmed by subcellular fractionation (**Supplementary Fig. 8g**). Furthermore, NK cells isolated from 5F8-treated tumors showed reduced cytosolic localization of pSTAT5 compared with that in cells isolated from control IgG-treated tumors (**Fig. 5c** and **Supplementary Fig. 8h**). pSTAT5 was partially colocalized with early endosome marker EEA1 (**Fig. 5d**), but not with late endosome marker LAMP1 (**Fig. 5e**), in DKK2-treated NK cells, which suggests that pSTAT5 may be sequestered

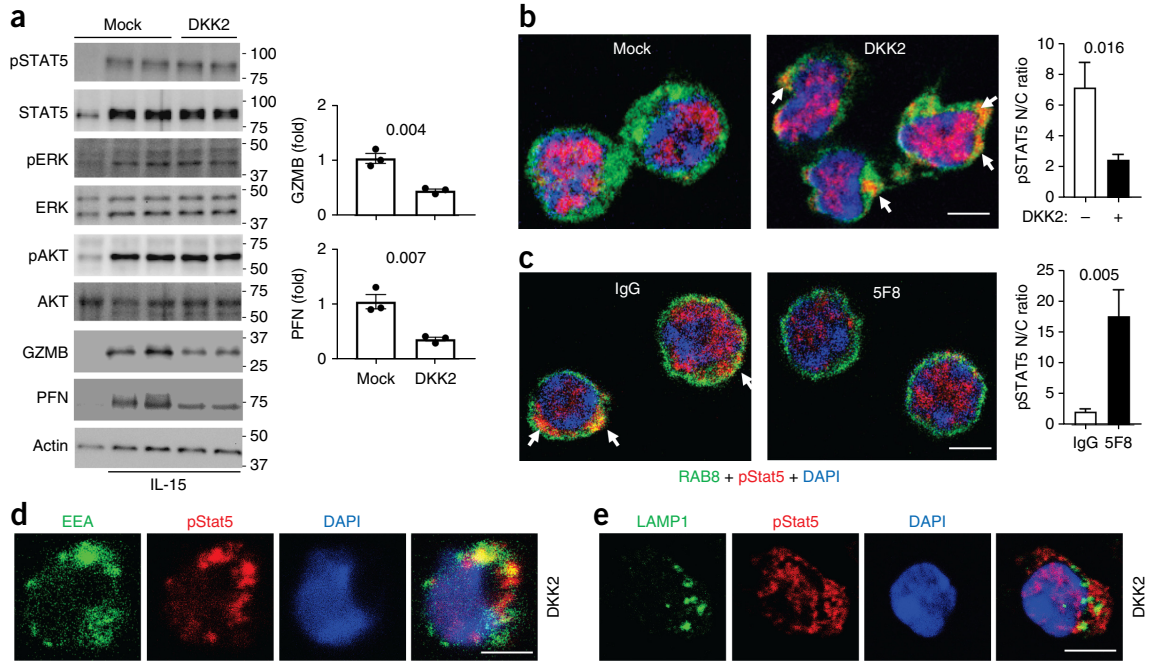

Figure 5 DKK2 impedes pSTAT5 nuclear localization. (**a**,**b**) Primary mouse NK cells were prepared and treated as in **Figure 4d**, and then subjected to western blotting analysis (**a**) or immunostaining with anti-pSTAT5, anti-RAB8 (as a cytosol marker), and DAPI, followed by Alexa Fluor 647 and FITC-labeled secondary antibodies (**b**). Individual color channels are shown in **Supplementary Figure 5f**. Western blots for GZMB and perforin and the nuclear-to-cytosol (N/C) ratio of pSTAT5 staining were quantified (two-sided Student's *t*-test; $n = 3$ for western blotting; $n = 15$ for staining). Uncropped western blots are provided in **Supplementary Figure 14**. (**c**) Tumor-infiltrating NK cells were isolated by FACS from MC38 tumors treated with IgG3 or 5F8 for 6 d (10 mg/kg injections). The cells were fixed, permeabilized, and stained with anti-RAB8, anti-pSTAT5, and DAPI, followed by Alexa Fluor 647 and FITC-labeled secondary antibodies. Individual color channels are shown in **Supplementary Figure 5h**. The N/C ratios of pSTAT5 staining were quantified (Student's *t*-test; $n = 15$). (**d**,**e**) Primary mouse NK cells were prepared and treated as in **a**, then immunostained with anti-pSTAT5, DAPI, and anti-EEA-1 (**d**) or anti-LAMP1 (**e**), followed by Alexa Fluor 647 and FITC-labeled secondary antibodies. Data are shown as mean ± s.e.m. with *P* values shown in plots, and experiments were repeated three times. Scale bars, 5 μm.

on early/recycling endosomes. Thus, we concluded that DKK2 treatment did not disrupt IL-15 signaling to STAT5 phosphorylation, but rather impaired the nuclear localization of pSTAT5.

DKK2 acts through LRP5, but not LRP6

DKK2 binds to LRP5 and LRP6. Although DKK2 inhibited the activation of primary NK cells that lacked LRP6 (**Supplementary Fig. 9a**), it did not inhibit LRP5-deficient NK cells (**Fig. 6a**). Additionally, DKK2 did not impair pSTAT5 nuclear localization in NK cells that lacked LRP5 (**Fig. 6b**). Thus, LRP5, but not LRP6, is required for DKK2's action on NK cells. The fact that LRP5 deficiency did not affect β-catenin accumulation stimulated by WNT3A in NK cells (**Supplementary Fig. 7b**) further confirms that the effect of the DKK2–LRP5 axis on NK activation is independent of Wnt–β-catenin signaling. LRP6 instead is required for Wnt–β-catenin signaling in NK cells, as WNT3A did not induce β-catenin accumulation in LRP6-deficient NK cells (**Supplementary Fig. 9b**).

We then tested the importance of LRP5 in tumor progression and the antitumor effect of DKK2 blockade by using hematopoietic-specific knockout of LRP5, which we accomplished by adoptive transfer of bone marrow from $Lrp5^{fl/fl}Mx1^{Cre}$ mice into lethally irradiated wild-type C57BL/6 mice. The lack of LRP5 in hematopoietic cells impaired MC38 tumor progression (**Fig. 6c**). We observed that 5F8 did not affect tumor progression in mice expressing mutant LRP5, whereas its effect was retained in the control mice (**Fig. 6c**). Flow cytometry analysis of tumor-infiltrating leukocytes supported the conclusion that 5F8 exerts its effects on cytotoxic immune cell activation via LRP5 (**Supplementary Fig. 9c**,**d**).

We also tested the importance of NK cell LRP5 in tumor progression and the antitumor effect of DKK2 blockade, using a mouse strain with NK-cell-specific LRP5 knockout ($Lrp5^{fl/fl}Ncr1$-Cre). MC38 tumors progressed more slowly in $Lrp5^{fl/fl}Ncr1$-Cre mice than in the control $Lrp5^{fl/fl}$ mice, and 5F8 showed marginal antitumor effects in these mice (**Supplementary Fig. 9e**). Concordantly, NK-cell-specific LRP5 knockout led to increased expression of NK cell activation markers, but had no effects on GZMB or CD69 in $CD8^+$ T cells (**Supplementary Fig. 9f**,**g**).

LRP5C interacts with and inhibits STAT5

To understand how LRP5 interferes with pSTAT5 nuclear localization, we carried out coimmunoprecipitation experiments, and found that LRP5 intracellular domain (LRP5C) interacted with STAT5 (**Fig. 6d**). We next found that LRP5C inhibited IL-15-mediated activation of STAT5 reporter gene activity in HEK293 cells expressing JAK3, IL-2/IL-15β and common γ-receptor subunits (**Fig. 6e**), without affecting STAT5 phosphorylation (**Fig. 6f**). LRP5C also inhibited STAT5 reporter gene activity stimulated by a constitutively active JAK1 mutant (V658F)[41] expressed in HEK293 cells without altering STAT5 phosphorylation, but it did impair the nuclear localization of pSTAT5 (**Fig. 6g**,**h**). These data are consistent with observations made in primary NK cells and support the conclusion that DKK2 inhibits IL-15 signaling by impeding the nuclear localization of pSTAT5, probably via LRP5C interaction with STAT5 as modeled in **Supplementary Figure 9h**. The observation that DKK2 induces rapid

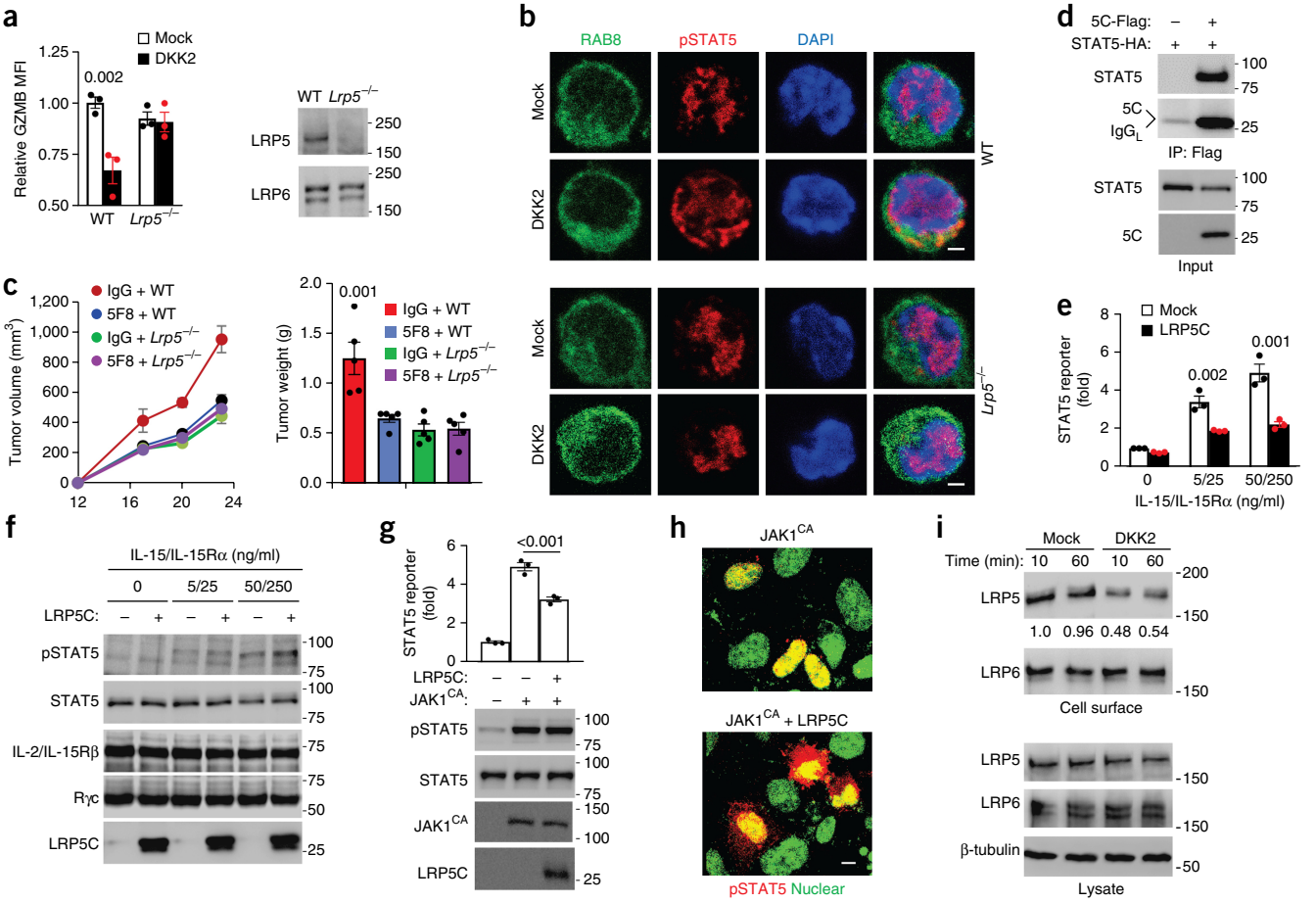

Figure 6 LRP5 is required for DKK2-mediated inhibition of NK cell activation. (**a**,**b**) Primary mouse NK cells were prepared from wild-type (WT) and *Lrp5*$^{-/-}$ mice, treated as in **Figure 4d**, and subjected to flow cytometry (two-way ANOVA) followed by western blotting analysis (**a**) and immunostaining (**b**). Immunostaining was done as in **Figure 5b**. MFI, mean fluorescence intensity. Scale bars, 2 μm. (**c**) C57BL/6 mice receiving *Lrp5*$^{fl/fl}$MX1^{Cre} (*Lrp5*$^{-/-}$) or *Lrp5*$^{fl/fl}$ (WT) bone marrow were treated with poly-I:C and then inoculated subcutaneously with MC38 cells. Treatment with 5F8 (10 mg/kg i.p.) was carried out at days 12, 16, and 20 after inoculation ($P < 0.01$ for tumor growth at days 20 and 24, IgG + WT versus 5F8 + WT; $P = 0.001$ for tumor weight in IgG + WT versus 5F8 + WT; $n = 5$; two-way ANOVA). (**d**) LRP5C and STAT5 coimmunoprecipitated in transfected HEK293 cells. HA, hemagglutinin. (**e**,**f**) HEK293 cells were infected with lentiviruses expressing JAK3, IL-2/IL-15Rβ, and the common γ-subunit (Rγc). The cells were then transfected with the plasmid for LRP5 intracellular domain (LRP5C), the STAT5-luc reporter gene, and RFP (internal control) for 24 h. The cells were stimulated with IL-15 and IL-15Rα-Fc for 6 h before the reporter gene assay (**e**; two-way ANOVA) and western blotting analysis (**f**). (**g**,**h**) HEK293 cells were cotransfected with the STAT5 reporter gene plasmid and plasmids for activated JAK1 (JAK1^{CA}, V658F) and LRP5C as indicated. After 24 h, the cells were analyzed for reporter gene activity (two-sided Student's *t*-test) or by western blotting (**g**) or immunostaining with anti-pSTAT5 and DAPI (**h**). Immunostained cells were examined by confocal microscope, and representative images are presented with pseudocolor. Scale bar, 8 μm. (**i**) HEK293 cells were treated with DKK2 for the indicated times. Biotinylated cell-surface proteins and cell-lysate proteins were analyzed by western blotting. The LRP5 blots were quantified and normalized against total LRP5. Uncropped western blots are provided in **Supplementary Figure 14**. Data are presented as mean ± s.e.m. with *P* values included in plots where relevant (**a**,**c**,**e**,**g**), and experiments were repeated three (**a**,**b**,**d**–**i**) or two (**c**) times.

internalization of LRP5 rather than LRP6 (**Fig. 6i**) provides a distinction between LRP5 and LRP6.

DKK2 suppresses tumor immune responses to anti-PD-1

We tested the combination of DKK2 blockade and PD-1 blockade in the MC38 tumor model. Although both PD-1 blockade and DKK2 blockade showed independent tumor-suppressive effects, the combination yielded further antitumor effects (**Supplementary Fig. 10a**,**b**). Notably, a small fraction of tumors subjected to the combination treatment showed long-term regression (**Supplementary Fig. 10a**). Flow analysis showed that individual blockades led to increased levels of GZMB in tumor-infiltrating CD8$^+$ T cells and NK cells, and that the combination blockade resulted in further increases in GZMB expression in these cells (**Supplementary Fig. 10c**,**d**). We carried out intratumoral administration of recombinant DKK2 protein to directly assess the effect of DKK2 on tumor immune responses elicited by PD-1 blockade. DKK2 inhibited PD-1-blockade-induced increases in the number of tumor-infiltrating CD45$^+$ T cells and CD8$^+$ T cells and the activation of CD8$^+$ T cells and NK cells (**Supplementary Fig. 10e**). These results suggest that DKK2 can suppress the effects of anti-PD-1 on immune effector cell activation. This conclusion is further supported by the observation that the effects of anti-PD-1 on tumor suppression and activation of tumor-infiltrated immune effector cells became insignificant in APC-null MC38-cell-derived tumors (**Supplementary Fig. 10f**,**g**), whereas DKK2 expression was upregulated (**Supplementary Fig. 1e**).

Analysis of the TCGA skin cutaneous melanoma cohort (provisional) revealed correlation of PTEN loss-of-function mutations

and PI3K gain-of-function mutations with elevated DKK2 expression (**Supplementary Fig. 11a**). These mutations lead to increased phosphatidylinositol-(3,4,5)-trisphosphate (PIP3) content in cells. In addition, a trend of correlation of PD-1 resistance with increased DKK2 expression (**Supplementary Fig. 11b**)[42] and significant correlation with PTEN-loss mutations[43] has been observed in human melanomas. We thus tested the antitumor effect of DKK2 blockade by using YUMM1.7 mouse melanoma cells. The YUMM1.7 cells were derived from *Braf*^{V600E}*Pten*$^{-/-}$*Cdkn2a*$^{-/-}$ melanoma developed in C57BL/6 mice[44]. The *Dkk2* mRNA content in YUMM1.7 cells, which was more than tenfold higher than that in MC38 cells, was reduced by the PI3K inhibitor wortmannin (**Supplementary Fig. 11c**), which suggests that DKK2 expression is regulated by PIP3. We observed that 5F8 impeded tumor progression and extended the survival of tumor-bearing mice in the YUMM1.7 tumor model (**Supplementary Fig. 11d**,**e**). Additionally, combined blockade of DKK2 and PD-1 outperformed blockade of only one or the other protein, with a fraction of combination-treated mice showing stable disease (**Supplementary Fig. 11d**,**e**). Flow analysis of tumor-infiltrating leukocytes showed notably stronger activation of CD8$^+$ T cells and NK cells by the combination blockade than by either individual blockade (**Supplementary Fig. 11f**). These data support the conclusion alluded to earlier that DKK2 can suppress antitumor immune responses elicited by PD-1 blockade.

Applicability of DKK2 blockade for treatment of other cancers

Activated *KRAS* mutations frequently occur in advanced human cancers. We tested DKK2 blockade in a mouse lung cancer model carrying an activating *Kras* mutation. The model was generated by intranasal administration of Cre-expressing adenovirus to *Apc*$^{fl/fl}$*Kras*$^{act/+}$ mice. Treatment of these mice with 5F8 significantly reduced tumor burden (**Supplementary Fig. 12a**) and increased the numbers and activation of CD8$^+$ T cells and NK cells (**Supplementary Fig. 12b**–**e**). These results, together with the correlation of high DKK2 expression with poor survival rates and of low GZMB expression with renal papillary carcinoma and bladder urothelial carcinoma revealed by the TCGA provisional database analysis (**Supplementary Fig. 13a**), suggest that DKK2 blockade may also be applicable to the treatment of cancers other than CRCs. Given that DKK2 is generally expressed at low levels in various normal human and mouse tissues, particularly immune tissues (http://www.ebi.ac.uk/gxa/home), DKK2 blockade is not likely to be a strong risk factor for autoimmunity. Indeed, neither DKK2 deficiency nor LRP5 deficiency altered various hematopoietic cell populations or NK cell development in mice housed under specific-pathogen-free conditions (**Supplementary Fig. 13b**–**e**). On the other hand, DKK2 may exert more potent effects on NK cells in tumors than those observed in our *in vitro* assays, as LRP5 expression was upregulated in tumor-infiltrating NK cells compared with that in primary NK cells from spleens (**Supplementary Fig. 13f**).

DISCUSSION

In this study, we uncovered a function of DKK2 in promoting tumor progression by suppressing NK cell and CD8$^+$ T cell activation in an LRP5-dependent manner. It remains unclear why LRP6 is not required for this DKK2 action. The ability of DKK2 to induce internalization of only LRP5 (**Fig. 6i**) may provide an explanation. DKK1 and WNT3A also fail to induce internalization of endogenous LRP6 (refs. 45,46). The three putative adaptor-protein-2-binding motifs in LRP5, in contrast to just one in LRP6, may underlie the difference in their internalization[46].

NK-cell-expressed STAT5 has direct roles in tumor immune surveillance[47]. On the basis of NK-cell-specific LRP5-knockout results, we believe that the DKK2-mediated impediment of STAT5 nuclear localization observed in this study is the primary mechanism for DKK2-mediated suppression of tumor immunity. DKK2 exerted a clear effect on STAT5 nuclear localization, but the effect was only partial (**Fig. 5b**). This partial effect may explain why DKK2 affects only NK cell activation, and not NK cell development, which in turn explains the lack of effect of DKK2 inhibition on NK cell numbers in mice, even though deficiency of STAT5 or IL-15Rα has a profound effect on NK cell development[48–50]. Thus, NK cell development and full activation may have different thresholds for STAT5 signaling.

DKK2 can also inhibit IL-15-mediated activation of CD8$^+$ T cells (**Supplementary Fig. 6d**), presumably through a similar mechanism. Of note, LRP5 expression is upregulated in human mature CD8$^+$ T cells[51], which suggests that DKK2 may also exert a stronger effect on CD8$^+$ T cells *in vivo*. However, DKK2 did not inhibit T-cell-receptor-mediated activation of primary T cells (data not shown). This explains the lack of an effect of DKK2 blockade on T cell populations. The activation of CD8$^+$ T cells by DKK2 blockade could also be a result of a combination of DKK2's direct and NK-cell-mediated indirect regulation of CD8$^+$ T cells[6,52,53]. Consistent with the prominent role of IL-15–STAT5 signaling in CD8$^+$ intraepithelial cells[11–13], DKK2 was able to inhibit CD8$^+$ IELs isolated from mouse intestines (**Supplementary Fig. 6e**). The direct inhibition of IELs by DKK2 may have a larger role in DKK2-blockade-associated increases in numbers of GZMB$^+$CD8$^+$ cells and tumor suppression in the *Apc*$^{Min/+}$ intestinal tumor model, which is consistent with the CD8$^+$ T cell depletion results (**Supplementary Fig. 5d**). Therefore, the potent antitumor effects of DKK2 blockade *in vivo* may be the results of its direct effects on NK cells and/or CD8$^+$ T cells, but the relative contributions of these mechanisms may be context dependent.

This study shows that APC loss drives DKK2 expression in CRCs, whereas PIP3-elevation mutations drive it in melanomas. We also found evidence that DKK2 provides resistance to PD-1 blockade in mouse models. These results suggest that DKK2 blockade may be used alone or in combination therapies to treat CRCs—the MSS CRCs in particular—and melanomas harboring PIP3-elevation mutations. DKK2 blockade may also be applied for the treatment of other human cancers in which DKK2 is expressed at high levels. These possibilities and the therapeutic potential of LRP5 blockade warrant future investigations.

METHODS

Methods, including statements of data availability and any associated accession codes and references, are available in the online version of the paper.

Note: Any Supplementary Information and Source Data files are available in the online version of the paper.

ACKNOWLEDGMENTS

We thank M. Orsulak for technical assistance and B. Williams (Van Andel Institute, Grand Rapids, Michigan, USA) for providing the LRP5/6 floxed mice. This work was supported by the NIH (grants GM112182 and CA214703 to D.W.), the Connecticut Bioscience Innovation Fund (to D.W.), NSFC (grant 31530094 to L.L.), the strategic priority research program of CAS (grant XDB19000000 to L.L.), and the CAS/SAFEA International Partnership Program for Creative Research Teams (to L.L. and D.W.).

AUTHOR CONTRIBUTIONS

D.W., L.L., Q.X., J.W., W.-J.W., W.T., M.S., and J.C. designed the experiments; Q.X., J.W., W.-J.W., S.C., Y.Z., M.S., W.T., and K.M. performed the experiments;

D.W., L.L., Q.X., W.-J.W., M.S., J.W., A.L.M.B., L.C., and W.T. analyzed the data; X.Y. performed statistic and bioinformatic analyses; M.B., V.S., and L.S. created and provided important reagents; D.W., L.L., Q.X., J.W., W.-J.W., and W.T. wrote the manuscript; and all authors reviewed and approved the manuscript.

COMPETING FINANCIAL INTERESTS

The authors declare competing financial interests: details are available in the online version of the paper.

1. Chen, D.S. & Mellman, I. Oncology meets immunology: the cancer-immunity cycle. *Immunity* **39**, 1–10 (2013).
2. Pardoll, D.M. The blockade of immune checkpoints in cancer immunotherapy. *Nat. Rev. Cancer* **12**, 252–264 (2012).
3. Postow, M.A., Callahan, M.K. & Wolchok, J.D. Immune checkpoint blockade in cancer therapy. *J. Clin. Oncol.* **33**, 1974–1982 (2015).
4. Coussens, L.M., Zitvogel, L. & Palucka, A.K. Neutralizing tumor-promoting chronic inflammation: a magic bullet? *Science* **339**, 286–291 (2013).
5. Topalian, S.L., Drake, C.G. & Pardoll, D.M. Immune checkpoint blockade: a common denominator approach to cancer therapy. *Cancer Cell* **27**, 450–461 (2015).
6. Palucka, A.K. & Coussens, L.M. The basis of oncoimmunology. *Cell* **164**, 1233–1247 (2016).
7. Topalian, S.L. *et al.* Safety, activity, and immune correlates of anti-PD-1 antibody in cancer. *N. Engl. J. Med.* **366**, 2443–2454 (2012).
8. Brahmer, J.R. *et al.* Safety and activity of anti-PD-L1 antibody in patients with advanced cancer. *N. Engl. J. Med.* **366**, 2455–2465 (2012).
9. Chung, K.Y. *et al.* Phase II study of the anti-cytotoxic T-lymphocyte-associated antigen 4 monoclonal antibody, tremelimumab, in patients with refractory metastatic colorectal cancer. *J. Clin. Oncol.* **28**, 3485–3490 (2010).
10. Sharma, P., Hu-Lieskovan, S., Wargo, J.A. & Ribas, A. Primary, adaptive, and acquired resistance to cancer immunotherapy. *Cell* **168**, 707–723 (2017).
11. Waldmann, T.A. The biology of interleukin-2 and interleukin-15: implications for cancer therapy and vaccine design. *Nat. Rev. Immunol.* **6**, 595–601 (2006).
12. Mishra, A., Sullivan, L. & Caligiuri, M.A. Molecular pathways: interleukin-15 signaling in health and in cancer. *Clin. Cancer Res.* **20**, 2044–2050 (2014).
13. Klose, C.S. *et al.* The transcription factor T-bet is induced by IL-15 and thymic agonist selection and controls CD8αα(+) intraepithelial lymphocyte development. *Immunity* **41**, 230–243 (2014).
14. Cheroutre, H., Lambolez, F. & Mucida, D. The light and dark sides of intestinal intraepithelial lymphocytes. *Nat. Rev. Immunol.* **11**, 445–456 (2011).
15. Jakobisiak, M., Golab, J. & Lasek, W. Interleukin 15 as a promising candidate for tumor immunotherapy. *Cytokine Growth Factor Rev.* **22**, 99–108 (2011).
16. Zarogoulidis, P. *et al.* Interleukin-7 and interleukin-15 for cancer. *J. Cancer* **5**, 765–773 (2014).
17. Hukelmann, J.L. *et al.* The cytotoxic T cell proteome and its shaping by the kinase mTOR. *Nat. Immunol.* **17**, 104–112 (2016).
18. Nandagopal, N., Ali, A.K., Komal, A.K. & Lee, S.H. The critical role of IL-15-PI3K-mTOR pathway in natural killer cell effector functions. *Front. Immunol.* **5**, 187 (2014).
19. Logan, C.Y. & Nusse, R. The Wnt signaling pathway in development and disease. *Annu. Rev. Cell Dev. Biol.* **20**, 781–810 (2004).
20. Moon, R.T., Kohn, A.D., De Ferrari, G.V. & Kaykas, A. WNT and beta-catenin signalling: diseases and therapies. *Nat. Rev. Genet.* **5**, 691–701 (2004).
21. MacDonald, B.T., Tamai, K. & He, X. Wnt/beta-catenin signaling: components, mechanisms, and diseases. *Dev. Cell* **17**, 9–26 (2009).
22. Clevers, H. & Nusse, R. Wnt/β-catenin signaling and disease. *Cell* **149**, 1192–1205 (2012).
23. Niehrs, C. The complex world of WNT receptor signalling. *Nat. Rev. Mol. Cell Biol.* **13**, 767–779 (2012).
24. Polakis, P. Wnt signaling in cancer. *Cold Spring Harb. Perspect. Biol.* **4**, a008052 (2012).
25. Niehrs, C. Function and biological roles of the Dickkopf family of Wnt modulators. *Oncogene* **25**, 7469–7481 (2006).
26. Bao, J., Zheng, J.J. & Wu, D. The structural basis of DKK-mediated inhibition of Wnt/LRP signaling. *Sci. Signal.* **5**, pe22 (2012).
27. Gage, P.J., Qian, M., Wu, D. & Rosenberg, K.I. The canonical Wnt signaling antagonist DKK2 is an essential effector of PITX2 function during normal eye development. *Dev. Biol.* **317**, 310–324 (2008).
28. Li, X. *et al.* Dkk2 has a role in terminal osteoblast differentiation and mineralized matrix formation. *Nat. Genet.* **37**, 945–952 (2005).
29. Mukhopadhyay, M. *et al.* Dkk2 plays an essential role in the corneal fate of the ocular surface epithelium. *Development* **133**, 2149–2154 (2006).
30. Li, X. *et al.* Chemical and genetic evidence for the involvement of Wnt antagonist Dickkopf2 in regulation of glucose metabolism. *Proc. Natl. Acad. Sci. USA* **109**, 11402–11407 (2012).
31. Wu, W., Glinka, A., Delius, H. & Niehrs, C. Mutual antagonism between dickkopf1 and dickkopf2 regulates Wnt/beta-catenin signalling. *Curr. Biol.* **10**, 1611–1614 (2000).
32. Li, L., Mao, J., Sun, L., Liu, W. & Wu, D. Second cysteine-rich domain of Dickkopf-2 activates canonical Wnt signaling pathway via LRP-6 independently of dishevelled. *J. Biol. Chem.* **277**, 5977–5981 (2002).
33. Caneparo, L. *et al.* Dickkopf-1 regulates gastrulation movements by coordinated modulation of Wnt/beta catenin and Wnt/PCP activities, through interaction with the Dally-like homolog Knypek. *Genes Dev.* **21**, 465–480 (2007).
34. Gaedcke, J. *et al.* Mutated *KRAS* results in overexpression of *DUSP4*, a MAP-kinase phosphatase, and *SMYD3*, a histone methyltransferase, in rectal carcinomas. *Genes Chromosom. Cancer* **49**, 1024–1034 (2010).
35. Matsui, A. *et al. DICKKOPF-4* and *-2* genes are upregulated in human colorectal cancer. *Cancer Sci.* **100**, 1923–1930 (2009).
36. Cancer Genome Atlas Network. Comprehensive molecular characterization of human colon and rectal cancer. *Nature* **487**, 330–337 (2012).
37. Su, L.K. *et al.* Multiple intestinal neoplasia caused by a mutation in the murine homolog of the APC gene. *Science* **256**, 668–670 (1992).
38. Afonina, I.S., Cullen, S.P. & Martin, S.J. Cytotoxic and non-cytotoxic roles of the CTL/NK protease granzyme B. *Immunol. Rev.* **235**, 105–116 (2010).
39. D'Amico, L. *et al.* Dickkopf-related protein 1 (Dkk1) regulates the accumulation and function of myeloid derived suppressor cells in cancer. *J. Exp. Med.* **213**, 827–840 (2016).
40. Malladi, S. *et al.* Metastatic latency and immune evasion through autocrine inhibition of WNT. *Cell* **165**, 45–60 (2016).
41. Haan, C. *et al.* Jak1 has a dominant role over Jak3 in signal transduction through γc-containing cytokine receptors. *Chem. Biol.* **18**, 314–323 (2011).
42. Hugo, W. *et al.* Genomic and transcriptomic features of response to anti-PD-1 therapy in metastatic melanoma. *Cell* **165**, 35–44 (2016).
43. Peng, W. *et al.* Loss of PTEN promotes resistance to T cell-mediated immunotherapy. *Cancer Discov.* **6**, 202–216 (2016).
44. Kaur, A. *et al.* sFRP2 in the aged microenvironment drives melanoma metastasis and therapy resistance. *Nature* **532**, 250–254 (2016).
45. Semënov, M.V., Zhang, X. & He, X. DKK1 antagonizes Wnt signaling without promotion of LRP6 internalization and degradation. *J. Biol. Chem.* **283**, 21427–21432 (2008).
46. Kim, I. *et al.* Clathrin and AP2 are required for PtdIns(4,5)P2-mediated formation of LRP6 signalosomes. *J. Cell Biol.* **200**, 419–428 (2013).
47. Gotthardt, D. *et al.* STAT5 is a key regulator in NK cells and acts as a molecular switch from tumor surveillance to tumor promotion. *Cancer Discov.* **6**, 414–429 (2016).
48. Imada, K. *et al.* Stat5b is essential for natural killer cell-mediated proliferation and cytolytic activity. *J. Exp. Med.* **188**, 2067–2074 (1998).
49. Teglund, S. *et al.* Stat5a and Stat5b proteins have essential and nonessential, or redundant, roles in cytokine responses. *Cell* **93**, 841–850 (1998).
50. Eckelhart, E. *et al.* A novel Ncr1-Cre mouse reveals the essential role of STAT5 for NK-cell survival and development. *Blood* **117**, 1565–1573 (2011).
51. Wu, B., Crampton, S.P. & Hughes, C.C. Wnt signaling induces matrix metalloproteinase expression and regulates T cell transmigration. *Immunity* **26**, 227–239 (2007).
52. Marcus, A. *et al.* Recognition of tumors by the innate immune system and natural killer cells. *Adv. Immunol.* **122**, 91–128 (2014).
53. Crouse, J., Xu, H.C., Lang, P.A. & Oxenius, A. NK cells regulating T cell responses: mechanisms and outcome. *Trends Immunol.* **36**, 49–58 (2015).

ONLINE METHODS

Mice. *Dkk2*$^{-/-}$ mice were described previously[28,30] and were back-crossed to the C57BL background for more than seven generations. *Ncr1*-Cre mice were also described previously[50]. NSG (NOD.Cg-Prkdc^{scid}Il2rg^{tm1Wjl}/SzJ), *Apc*$^{Min/+}$ (C57BL/6J-ApcMin/J), MX1^{Cre} (B6.Cg-Tg(Mx1-cre)1Cgn/J), *Kras*$^{LSL-G12D}$ (B6.129S4-Krastm4Tyj/J), and *Apc*$^{fl/fl}$ (C57BL/6-Apctm1Tyj/J) mice were acquired from the Jackson Laboratory. Wild-type C57BL/6 mice were purchased from Envigo (Harlan). The LoxP-floxed *Lrp5* (*Lrp5*$^{fl/fl}$) and *Lrp6* (*Lrp6*$^{fl/fl}$) mice were obtained from Bart Williams[54]. The *Lrp5*$^{fl/fl}$ and *Lrp6*$^{fl/fl}$ mice were back-crossed with C57BL/6 mice for more than seven generations before being intercrossed with MX1^{Cre} mice. *Lrp5* and *Lrp6* gene disruption was induced by intraperitoneal injection of 40 µl of poly-I:C (10 mg/mL) into the *Lrp5*$^{fl/fl}$MX1^{Cre} mice every other day for four treatments. The mice were used for NK cell isolation 3 weeks after the poly-I:C treatment. For adoptive bone marrow transfer, bone marrow from *Lrp5*$^{fl/fl}$MX1^{Cre} mice was transferred into lethally irradiated C57BL/6 mice (8-week-old females) via retro-orbital injection. After recovery (8 weeks), the mice were treated with poly-I:C and used in experiments 3 weeks after poly-I:C treatment. Mice were housed in specific-pathogen-free conditions and cared for in accordance with US National Institutes of Health guidelines, and all procedures were approved by the Yale University Animal Care and Use Committee.

Antibodies and cells. We used antibodies to pSTAT5 (Tyr694) (CST, 4322s), LAMP1 (sc-19992, Santa Cruz), EEA1 (BD Bioscience, 612006), phospho-AKT (serine 473) (CST, 4060), AKT1 (CST, 9272), phospho-ERK1/2 (Thr202/Tyr204) (CST, 4377), ERK1/2 (CST 9102), perforin (CST, 3693), granzyme B (CST, 4275), β-actin (CST, 3700), Flag (Sigma Aldrich, F3165), β-catenin (BD Bioscience, 610153), LRP5 (CST, 5731), LRP6 (CST, 3395), mouse CD4–PE (eBioscience, 12-0042-82), mouse NK1.1–allophycocyanin (BioLegend, 108710), mouse CD8a–PE–cyanine 7 (eBioscience, 25-0081-82), mouse CD69–PE (Biolegend, 104508), human/mouse granzyme B–FITC (BioLegend, 515403), mouse CD314 (NKG2D)–PE–cyanine 7 (eBioscience, 25-5882-81), mouse CD3e–PE (eBioscience, 12-0031-82), mouse IFN-γ–PE (eBioscience, 12-7311-81), CTLA-4/CD152 (1B8)–FITC (Thermo Fisher, HMCD15201), human CD45–eFluor 450 (eBioscience, 48-0459-41), mouse CD107a–V450 (BD, 560648), mouse CD8a–allophycocyanin (eBioscience, 17-0081-81), mouse CD25–Alexa Fluor 488 (eBioscience, 53-0251-82), mouse CD279 (PD-1)–PE (BioLegend, 135205), mouse CD19–PE–cyanine 7 (eBioscience, 25-0193-81), mouse CD3e–eFluor 450 (eBioscience, 48-0031-82), mouse CD11b–PE (eBioscience, 12-0112-82), mouse CD27–FITC (eBioscience, 11-0271-82), Ki67 (Abcam, ab15580), cleaved caspase-3 (Asp175) (CST, 9661S), CD31 (Abcam ab, 28364), CD44 (Abcam, ab157107), FITC-labeled AffiniPure F(ab)$_2$ fragment donkey anti-mouse IgG (H+L) (Jackson Lab, 715-096-151), mouse integrin $\alpha_4\beta_7$ (LPAM-1)–allophycocyanin (eBioscience, 17-5887-80), human CD56 (NCAM)–allophycocyanin (eBioscience, 17-0566-41), human CD16–PE (eBioscience, 12-0167-42), human CD3–eFluor 450 (eBioscience, 48-0037-42), and Alexa Fluor 647–labeled AffiniPure F(ab)$_2$ fragment goat anti-rabbit IgG (H+L) (Jackson Lab, 111-606-045). Mouse monoclonal antibody (mAb) to DKK2 (5F8) was generated by standard hybridoma technology through immunization of mice with a synthetic peptide (KLNSIKSSLGGETPGC) of human DKK2 at AbMax (Beijing, China). Therapeutic antibodies to PD-1 were hamster mAb clone G4 (ref. 55) and Clone J43 (BioXcell, BP0033-2) with polyclonal Armenian hamster IgG (BioXcell, BE0091) as the control IgG.

HEK293 and HCT-116 cells were purchased from ATCC. YUMM1.7 was provided by M.B. and was reported previously[44]. MC38 was purchased from Kerafast (Boston, MA). Cells were all tested for mycoplasma and were shown to be negative.

Quantitative RT-PCR. Total RNAs were isolated from cells with the RNeasy Plus mini kit (Qiagen). Complementary DNAs were synthesized from the RNAs with the iScript cDNA synthesis kit (Bio-Rad). Quantitative PCR was done with iTaq Universal SYBR Green Supermix (Bio-Rad). The primer sequences are listed in **Supplementary Table 2**. The intestinal epithelial stem cell and differentiation markers were selected on the basis of information in refs. 56–59.

ELISA. Recombinant mouse DKK2 or DKK1 protein (20 ng/ml; R&D) in a blocking buffer (1% BSA in PBS) was incubated in a 384-well microtiter plate overnight at 4 °C. The plate was washed with PBS twice and incubated with the blocking buffer for 1 h at room temperature. The plate was then incubated with the 5F8 antibody in the blocking buffer for 1 h at room temperature. After repeated washing, the plate was incubated with an HRP-conjugated secondary antibody for 1 h at room temperature. A chemiluminescent substrate (Thermo Fisher, 37070) was added to the plate, and the plate was read by an EnVision plate reader.

DKK2-AP binding assay. The binding assay was performed as previously described[60]. In brief, HEK293 cells were transfected with LacZ or LRP5 using Lipofectamine Plus for 24 h. Cells were washed once with a cold washing buffer (Hanks' buffered salt solution containing 1% bovine serum albumin, 20 mM HEPES, and 0.5% NaN_3) and incubated with washing buffer containing 20% DKK2-AP conditioned medium on ice for 2 h. The cells were then washed three times with the washing buffer and lysed with 1% Triton X-100 and 20 mM Tris-HCl, pH 7.5. The lysates were heated at 65 °C for 10 min to inactivate endogenous AP and then added with a chemiluminescence AP substrate (Thermo Fisher, T1015). The activity was measured by an EnVision plate reader.

Tumor graft. MC38 or YUMM1.7 melanoma tumor cells ($0.5–1 \times 10^6$) were mixed with BD Matrigel (Matrix Growth Factor Reduced) (BD, 354230) in 100 µl and injected subcutaneously into the right flanks of the backs of female C57BL mice (8–10 weeks old). Tumor growth was measured with calipers, and size was expressed as one-half of the product of perpendicular length and square width in cubic millimeters. For antibody treatment, control IgG3 antibody and anti-DKK2 were diluted in PBS, and 100 µl was injected intraperitoneally (i.p.) at the intervals indicated in the figures. For survival tests, mice were euthanized when the tumor size exceeded 1,500 mm^3 for MC38 and 1,200 mm^3 for YUMM1.7.

Preparation of tumor-infiltrating leukocytes. Tumors were minced with scissors and scalpel blades and incubated with digestion buffer (RPMI 1640 medium, 5% FBS, 1% penicillin—streptomycin, 25 mM HEPES, and 300 U collagenase (Sigma C0130)) in a shaker for 2 h at 37 °C. Disperse cells were filtered through a 70-µm cell strainer to eliminate clumps and debris. After centrifugation for 5 min (500*g*) at 4 °C, cell pellets were resuspended in red blood cell lysis buffer (Sigma R7757) and incubated at room temperature for 5 min to remove erythrocytes. Cells were pelleted again, resuspended, and incubated in 0.05% Trypsin/EDTA at 37 °C for 5 min, after which they underwent DNA digestion with the addition of type I DNase (1 µg/ml final; Sigma, D4263) for 5 min. Trypsin digestion was stopped by the addition of FBS to 5%, and cells were filtered again through a 40-µm cell strainer. Finally, the cells were pelleted again and resuspended in PBS at a concentration of 2×10^7.

Flow cytometry. Cells in single-cell suspension were fixed with 2% PFA (Santa Cruz, sc-281692). After being washed with a flow cytometry staining buffer (eBioscience, 00-4222-26), cells were stained with antibodies for cell-surface markers for 1 h on ice in the dark. For staining of intracellular proteins, the cells were washed and resuspended in permeabilization buffer (BD, 554723) and stained by antibodies in the permeabilization buffer for 1 h on ice in the dark. The cells were then pelleted and resuspended in the flow cytometry staining buffer for flow cytometry analysis.

Tumor sectioning and immunostaining. Tissues were fixed with 4% PFA (Santa Cruz, sc-281692) for 4–6 h on a shaker at 4 °C. They were then washed with PBS three times and perfused in 20% sucrose solution in PBS overnight at 4 °C. They were subsequently mounted in OCT embedding compound and frozen first at –20 °C and then at –80 °C. Tissue sections were prepared at 8-µm thickness with a cryostat and mounted onto gelatin-coated histological slides, which were stored at –80 °C.

For immunostaining, slides were thawed to room temperature and fixed in pre-cold acetone for 10 min, then rehydrated in PBS for 10 min. The slides were incubated in a blocking buffer (1% horse serum and 0.02% Tween 20 in PBS) for 1–2 h at room temperature, then incubated with primary antibodies, which were diluted in the blocking buffer, overnight at 4 °C. The slides were then washed three times with PBS and incubated with a secondary antibody (donkey

anti-rabbit IgG H&L (DyLight 550) preadsorbed (Abcam, ab96920)) in the incubation buffer for 1 h at room temperature. After repeated washes, the slides were mounted with an anti-fade mounting media containing DAPI (Thermo Fisher, P36931) and visualized with a confocal microscope.

Cytotoxic effector immune cell depletion. For depletion of NK cells with the MC38 model, anti-NK1.1 (PK136, BioXcell BE0036) or isotype control antibody (BioXcell BE0085) was injected i.p. at 300 μg per mouse on days −1, 5, 11 and 17 relative to tumor cell inoculation. For CD8 depletion, anti-CD8α (YTS169.4, BioXcell BE0117) or isotype control antibody (Clone LTF-2, BioXcell BE0090) was injected i.p. at 300 μg per mouse at days 12, 15, and 19 after tumor cell inoculation.

For the $Apc^{Min/+}$ model, $NK1.1^+$ and $CD8^+$ T cells were depleted by i.p. injection of 10 mg/kg anti-NK1.1 (PK136, BioXcell BE0036) and anti-CD8α (YTS169.4, BioXcell BE0117), respectively. Male $Apc^{Min/+}$ mice were treated weekly with the control IgG3 antibody or 5F8 (8 mg/kg) starting at the age of 15 weeks. The depletion antibodies were given 6 d before the therapeutic treatment at an interval of 5 d. The mice were examined 4 weeks after the treatment.

Preparation and treatment of mouse primary NK cells, $CD8^+$ T cells and IELs. Mouse primary NK cells and $CD8^+$ T cells were isolated from the spleens of female mice (8 weeks old) with NK cell and $CD8^+$ T cell isolation kits according to the manufacturer's instructions (Miltenyi Biotec #130-090-864 and #130-104-075, respectively). Primary NK cells were cultured in RPMI 1640 medium (Gibco, 11875-093) supplemented with 10% FBS, penicillin (100 U/ml), streptomycin (100 μg/ml), 2-mercaptoethanol (500 μM), and HEPES (10 mM) at 37 °C supplemented with 5% CO_2 in the presence of recombinant murine IL-15 (50 ng/ml) for 24 h before treatment with DKK2, CHIR99021, or WNT3A. $CD8^+$ T cells were cultured in the same culture medium and conditions as NK cells, but were supplemented with IL-15 (200 ng/ml) and IL-15Rα (1 μg/ml recombinant mouse IL-15 receptor-α Fc chimera protein from R&D) for 96 h before DKK2 treatment.

Mouse primary IELs were prepared as described in refs. 61,62. In brief, the small intestine was everted, divided into four pieces, and washed twice in PBS containing 100 U/ml penicillin–streptomycin. The specimens were then incubated with stirring at 37 °C in prewarmed Ca^{2+}- and Mg^{2+}-free Hanks' solution containing 100 U/ml penicillin–streptomycin, 5% FCS, 2 mM dithiothreitol, and 5 mM EDTA for 30 min, and then shaken vigorously for 30 s. The supernatants were passed over two nylon wool columns to remove undigested tissue debris. The lymphocytes obtained were pooled and enriched on a discontinuous (40% and 70%) Percoll density gradient. Cells at the interface between the 40% and 70% fractions (IELs) were collected for treatment with IL-15 (200 ng/ml) and DKK2 (400 ng/ml), and then subjected to flow analysis.

Preparation of human NK cells. Peripheral blood mononuclear cells from healthy humans were purchased from ZenBio (SER-PBMC-200). Human NK cells were isolated from the PBMCs with a human NK cell isolation kit according to the manufacturer's instruction (Miltenyi Biotec, #130-092-657). Human NK cells were cultured in RPMI 1640 medium (Gibco, 11875-093) supplemented with 10% heat-inactivated FBS, penicillin (100 U/ml), streptomycin (100 μg/ml), 2-mercaptoethanol (500 μM), and HEPES (10 mM) at 37 °C, supplemented with 5% CO_2, in the presence of recombinant human IL-15 (50 ng/ml) before treatment with recombinant human DKK2 protein.

NK cell and tumor cell coculture. Primary NK cells were isolated from spleens as described above and cultured in the presence of 50 ng/ml recombinant murine IL-15 for 24 h. Meanwhile, tumor cells were plated in a 96-well plate and left overnight. NK cells were added into the tumor cells at a 7:1 ratio in the presence of the IgG3 antibody or anti-mDKK2 5F8 for 9 h at 37 °C. To test the effect of DKK2 in coculture, we cultured isolated NK cells in the presence of 50 ng/ml recombinant murine IL-15 for 24 h and then in the presence or absence of DKK2 for another 24 h before adding the NK cells to pre-seeded MC38 cells at a 7:1 (NK:MC38) ratio. The numbers of live tumor cells were determined by a Guava flow cytometer (EMD Millipore), whereas the cell apoptosis was assessed by flow cytometry with an annexin V apoptosis detection kit (eBioscience, 88-8007).

Immunocytostaining. Primary NK cells were prepared as described above and treated as indicated in the figures. They were then placed on poly-lysine-coated coverslips and incubated for 30 min at room temperature. HEK293 cells grown on coverslips were transfected and stimulated as indicated in the figures. Cells were fixed with 4% PFA for 10 min at room temperature and permeabilized with ice-cold methanol for 10 min at −20 °C. After being rinsed with PBS three times, cells were blocked with a blocking buffer (5% normal donkey serum and 0.5% Triton in PBS) for 1 h at room temperature. Primary antibodies were then diluted in PBS with 0.5% BSA and applied to cells for overnight incubation at 4 °C. Cells were rinsed with PBS three times and incubated with diluted fluorochrome-conjugated secondary antibodies (in PBS with 1% BSA) for 1 h at room temperature. Finally, cells were rinsed with PBS three times and mounted with Prolong Gold Antifade solution (Thermo Fisher) for confocal microscopy.

For quantification of subcellular localization, we determined the nuclear/cytoplasmic ratio of pSTAT5 staining intensities. The staining intensities of pSTAT5 in the nuclei, which were delineated by DAPI staining, and in the cytosol, which was delineated by RAB8 staining, were quantified in ImageJ.

Immunoprecipitation. 293T cells were transfected with plasmids encoding STAT5 and/or LRP5C–Flag with Lipofectamine Plus. The cells were lysed 24 h after transfection in lysis buffer (50 mM HEPES, pH 7.4, 150 mM NaCl, 1% Triton X-100, 10% glycerol, 2 mM $MgCl_2$, 2 mM EGTA) with protease inhibitor cocktail (Roche) and phosphatase inhibitors (Phospo-stop; Roche) on ice. Cell lysates were centrifuged to remove insoluble materials. Immunoprecipitation was performed with anti-Flag overnight, and was followed by 2-h incubation with Protein-A/G Plus beads (Santa Cruz) at 4 °C. The beads were washed repeatedly, and bound proteins were analyzed by western blotting.

Reporter gene assays. The STAT5 reporter gene assays were done in HEK293 cells for activated JAK1-induced activity or in those stably expressing JAK3, IL-2/IL-15Rβ and the common receptor γ-subunit for IL-15-induced activity. Cells were seeded at 8×10^4 cells per well in a 48-well plate. The next day, cells were transfected by Lipofectamine 2000 (Invitrogen) with pGL4.52-STAT5-luciferase (Promega) and tagRFP (internal control) plasmids together with other plasmids expressing genes of interest. The total amount of plasmid was kept at 125 ng per well. The cells were added 24 h after transfection with IL-15/IL-15Rα–Fc complex or mock. Six hours later, the cells were lysed and subjected to RFP fluorescence and luciferase luminescence measurement by an Envision plate reader. The reporter gene activity presented is normalized against RFP readings.

The Wnt reporter gene assay was carried out in HEK293 cells that were transfected with TOPFlash and GFP plasmids. The rest of the protocol was the same as described above. The reporter gene activity presented is normalized against GFP readings.

Generation of APC-mutant cells. Gene editing of the APC genes in MC38 and HCT116 cells was done via the CRISPR–Cas9 system as previously described[63]. The cells were transfected with two Cas9 plasmids expressing two guiding RNAs targeted to the gene encoding APC. This caused homozygous C-terminal deletion of the APC protein starting at Gly855 in MC38 cells. As these two guiding RNAs were coexpressed with GFP or RFP, respectively, the GFP^+RFP^+ cells were sorted directly into 96-well plates at a density of 1.2 cells per well. Homozygous mutations in *APC* or *Apc* were detected by PCR and confirmed by DNA sequencing. Positive clones were pooled to avoid clonal effects. The guiding and PCR sequences are listed in **Supplementary Table 2**.

LRP5/6 internalization assay. HEK293 cells were treated with mock or recombinant mouse DKK2 protein (250 ng/ml) in culture medium for the durations indicated in the figures. The cells were washed with pre-cold PBS, and cell-surface proteins were biotinylated with 0.5 mg/ml EZ-Link Sulfo-NHS-SS-Biotin (Thermo Fisher, 21445) in a PBS buffer on ice for 30 min. The reaction was stopped by the addition of PBS containing ice-cold 50 mM NH_4Cl, followed by repeated washes with ice-cold PBS. The cells were then lysed in a buffer containing 1.25% Triton X-100, 0.25% SDS, 50 mM Tris-HCl, pH 8.0, 150 mM NaCl, 5 mM EDTA, 5 mg/ml iodoacetamide, 10 μg/ml PMSF, and the Roche proteinase inhibitor cocktail. After centrifugation, aliquots were taken as lysate controls,

doi:10.1038/nm.4496

and the rest of supernatants were used in pulldowns with NeutrAvidin beads (Thermo Fisher, 29200) followed by western blotting analysis.

Cell fractionation. Cell fractionation was carried out with the cell fractionation kit from Cell Signaling Technology (#9038) according to the manufacturer's protocol. In brief, primary NK cells (2 million) were washed with cold PBS and resuspended in cytoplasm isolation buffer. After centrifugation, the supernatant was collected as the cytosol fraction and the pellet was resuspended in membrane isolation buffer. After centrifugation, the supernatant was collected with the membrane fraction, whereas the pellet was collected as the nuclear fraction. The nuclear fraction and the pool of the membrane and cytosolic fractions were subjected to western blotting analysis.

RNA sequencing and data analysis. Primary NK cells were isolated from spleens as described above and cultured in the presence of 50 ng/ml recombinant murine IL-15 for 24 h and then cultured in the presence or absence of 500 ng/ml DKK2 for another 24 h before mRNA was isolated and purified with the RNeasy Plus mini kit (Qiagen). RNA-seq libraries were prepared with the TrueSeq stranded total RNA library prep kit (Illumina) and sequenced on an Illumina HiSeq 2500 with 50-base single-end reads.

Raw sequence reads were mapped with TopHat in Galaxy (Version 2.1.0) with ENCODE annotation M1. The raw counts were then normalized via the trimmed mean of M values (TMM) method and compared using the Bioconductor package edgeR. Reads per kilobase per million mapped reads (RPKM) were also calculated from the raw counts and have been deposited at GEO (GSE100402). Differentially expressed genes were identified if RPKM ≥ 1 in at least one sample, and fold change was ≥1.25. Pathway analysis of RNA-sequencing results was performed with Enrichr (http://amp.pharm.mssm.edu/Enrichr). Gene enrichment analysis was performed with Motif Gene Set (http://software.broadinstitute.org/gsea/msigdb/index.jsp)[64].

***In situ* hybridization.** *In situ* hybridization detection of *Dkk2* mRNA was carried out with the following reagents acquired from Advanced Cell Diagnostics, using the provided protocol: RNAscope Target Retrieval Reagents (322000), RNAscope Pretreat Reagents-H202 and ProteasePlus (322330), RNAscope 2.5 HD Detection Reagent—RED (322360), RNAscope Wash Buffer Reagents (310091), BioCare EcoMount (320409), ImmECatdge Hydrophobic Barrier Pen (310018), and the mouse *Dkk2* probe (404841).

Correlation of DKK2 expression and survival. Data on DKK2 expression, overall survival, and relapse-free survival were obtained from the TCGA provisional data sets as of 20 July 2016. The high and low DKK2 expressers were grouped on the basis of an arbitrary cutoff percentile of 15%. Mantel–Cox log-rank tests were done using the GraphPad Prism 7 software.

Statistical analysis and study design. Minimal group sizes for tumor-progression studies were determined via power calculations with the DSS Researcher's Tookit with an α of 0.05 and power of 0.8. Animals were grouped unblinded, but randomized, and investigators were blinded for the qualification experiments. No samples or animals were excluded from analysis. Assumptions concerning the data including normal distribution and similar variation between experimental groups were examined for appropriateness before statistical tests were conducted. Comparisons between two groups were performed by unpaired, two tailed *t*-test. Comparisons between more than two groups were performed by one-way ANOVA, whereas comparisons with two or more independent variable factors were performed by two-way ANOVA followed by Bonferroni's *post hoc* correction using Prism 6.0 software (GraphPad). Statistical tests were done with biological replicates. $P < 0.05$ was considered statistically significant.

Life Sciences Reporting Summary. Further information on experimental design and reagents is available in the **Life Sciences Reporting Summary**.

Data availability. The raw RNA-seq data are available in the NCBI Gene Expression Omnibus (GSE100402).

54. Cui, Y. *et al.* Lrp5 functions in bone to regulate bone mass. *Nat. Med.* **17**, 684–691 (2011).
55. Hirano, F. *et al.* Blockade of B7-H1 and PD-1 by monoclonal antibodies potentiates cancer therapeutic immunity. *Cancer Res.* **65**, 1089–1096 (2005).
56. Belov, L., Zhou, J. & Christopherson, R.I. Cell surface markers in colorectal cancer prognosis. *Int. J. Mol. Sci.* **12**, 78–113 (2010).
57. Sansom, O.J. *et al.* Loss of Apc in vivo immediately perturbs Wnt signaling, differentiation, and migration. *Genes Dev.* **18**, 1385–1390 (2004).
58. Sarraf, P. *et al.* Differentiation and reversal of malignant changes in colon cancer through PPARγ. *Nat. Med.* **4**, 1046–1052 (1998).
59. Vermeulen, L. & Snippert, H.J. Stem cell dynamics in homeostasis and cancer of the intestine. *Nat. Rev. Cancer* **14**, 468–480 (2014).
60. Wang, K. *et al.* Characterization of the Kremen-binding site on Dkk1 and elucidation of the role of Kremen in Dkk-mediated Wnt antagonism. *J. Biol. Chem.* **283**, 23371–23375 (2008).
61. Little, M.C., Bell, L.V., Cliffe, L.J. & Else, K.J. The characterization of intraepithelial lymphocytes, lamina propria leukocytes, and isolated lymphoid follicles in the large intestine of mice infected with the intestinal nematode parasite *Trichuris muris*. *J. Immunol.* **175**, 6713–6722 (2005).
62. Li, Z. *et al.* Small intestinal intraepithelial lymphocytes expressing CD8 and T cell receptor γδ are involved in bacterial clearance during *Salmonella enterica* serovar *Typhimurium* infection. *Infect. Immun.* **80**, 565–574 (2012).
63. Ran, F.A. *et al.* Genome engineering using the CRISPR-Cas9 system. *Nat. Protoc.* **8**, 2281–2308 (2013).
64. Subramanian, A. *et al.* Gene set enrichment analysis: a knowledge-based approach for interpreting genome-wide expression profiles. *Proc. Natl. Acad. Sci. USA* **102**, 15545–15550 (2005).

nature research

Corresponding author(s): Dianqing Wu

Life Sciences Reporting Summary

Nature Research wishes to improve the reproducibility of the work that we publish. This form is intended for publication with all accepted life science papers and provides structure for consistency and transparency in reporting. Every life science submission will use this form; some list items might not apply to an individual manuscript, but all fields must be completed for clarity.

For further information on the points included in this form, see Reporting Life Sciences Research. For further information on Nature Research policies, including our data availability policy, see Authors & Referees and the Editorial Policy Checklist.

Please do not complete any field with "not applicable" or n/a. Refer to the help text for what text to use if an item is not relevant to your study.
For final submission: please carefully check your responses for accuracy; you will not be able to make changes later.

Experimental design

1. Sample size

Describe how sample size was determined.

Minimal group sizes for tumor progression studies were determined by using power calculations with the DSS Researcher's Tookit with an α of 0.05 and power of 0.8.

2. Data exclusions

Describe any data exclusions.

No data were excluded from analysis.

3. Replication

Describe the measures taken to verify the reproducibility of the experimental findings.

All attempts at replication were successful.

4. Randomization

Describe how samples/organisms/participants were allocated into experimental groups.

All mice were randomly assigned to experimental groups.

5. Blinding

Describe whether the investigators were blinded to group allocation during data collection and/or analysis.

Animals were grouped unblinded, but investigators were blinded for most of the qualification experiments.

Note: all in vivo studies must report how sample size was determined and whether blinding and randomization were used.

6. Statistical parameters

For all figures and tables that use statistical methods, confirm that the following items are present in relevant figure legends (or in the Methods section if additional space is needed).

n/a	Confirmed
☐	☒ The exact sample size (*n*) for each experimental group/condition, given as a discrete number and unit of measurement (animals, litters, cultures, etc.)
☐	☒ A description of how samples were collected, noting whether measurements were taken from distinct samples or whether the same sample was measured repeatedly
☐	☒ A statement indicating how many times each experiment was replicated
☐	☒ The statistical test(s) used and whether they are one- or two-sided *Only common tests should be described solely by name; describe more complex techniques in the Methods section.*
☐	☒ A description of any assumptions or corrections, such as an adjustment for multiple comparisons
☐	☒ Test values indicating whether an effect is present *Provide confidence intervals or give results of significance tests (e.g. P values) as exact values whenever appropriate and with effect sizes noted.*
☐	☒ A clear description of statistics including central tendency (e.g. median, mean) and variation (e.g. standard deviation, interquartile range)
☐	☒ Clearly defined error bars in all relevant figure captions (with explicit mention of central tendency and variation)

See the web collection on statistics for biologists for further resources and guidance.

Nature Medicine: doi:10.1038/nm.4496

Software

Policy information about availability of computer code

7. Software

Describe the software used to analyze the data in this study.

Statistical analyses were performed using GraphPad Prism 7.0. ImageJ was used for biochemical analysis of Western blots. RNA-seq was analyzed with TopHat in Galaxy (Version 2.1.0) with ENCODE annotation M1 and the Bioconductor package "edgeR".

For manuscripts utilizing custom algorithms or software that are central to the paper but not yet described in the published literature, software must be made available to editors and reviewers upon request. We strongly encourage code deposition in a community repository (e.g. GitHub). *Nature Methods* guidance for providing algorithms and software for publication provides further information on this topic.

Materials and reagents

Policy information about availability of materials

8. Materials availability

Indicate whether there are restrictions on availability of unique materials or if these materials are only available for distribution by a third party.

NO restrictions on availability of materials.

9. Antibodies

Describe the antibodies used and how they were validated for use in the system under study (i.e. assay and species).

Antibodies used for flow cytometry include: V450 Mouse Anti-Mouse CD45.2 (BD Horizon, 560697, Clone 104), V450 Rat Anti-Mouse CD107a (BD Horizon, 560648, Clone 1D4B), PE/Cy7 anti-mouse CD45.2 Antibody (BioLegend,109830,clone 104), APC anti-mouse NK-1.1 Antibody (BioLegend,108710,clone PK136), APC anti-mouse CD49b (pan-NK cells) Antibody (BioLegend, 108910, clone DX5), FITC anti-human/mouse Granzyme B Antibody (BioLegend,515403,clone GB11), Alexa Fluor¨ 647 anti-human/mouse Granzyme B Antibody (BioLegend,515406,clone GB11), Pacific Blueª anti-mouse CD8a Antibody (BioLegend,100725,clone 53-6.7),PE anti-mouse CD69 Antibody (BioLegend,104508,clone H1.2F3), PE anti-mouse CD279 (PD-1) Antibody (BioLegend,135205,clone 29F.1A12), PE anti-human CD69 Antibody (BioLegend,310906,clone FN50), PE anti-human IFN-γ Antibody (BioLegend,506507,clone B27), APC anti-human IFN-γ Antibody (BioLegend,502512,clone 4S.B3), IFN gamma Monoclonal Antibody (XMG1.2), PE (eBioscience,12-7311-82,clone XMG1.2), CD314 (NKG2D) Monoclonal Antibody (CX5), PE-Cyanine7 (eBioscience,25-5882-82,clone CX5), CD8a Monoclonal Antibody (53-6.7), PE-Cyanine7 (eBioscience,25-0081-82,clone 53-6.7), CD8a Monoclonal Antibody (53-6.7), APC (eBioscience,17-0081-82,clone 53-6.7), CD4 Monoclonal Antibody (RM4-5), PE (eBioscience,12-0042-82,clone RM4-5), CD44 Monoclonal Antibody (IM7), PE-Cyanine7 (eBioscience,25-0441-81,clone IM7), CD62L (L-Selectin) Monoclonal Antibody (MEL-14), APC (eBioscience,17-0621-81,clone MEL-14), Integrin alpha 4 beta 7 (LPAM-1) Monoclonal Antibody (DATK32 (DATK-32)), APC (eBioscience,17-5887-80,clone DATK32 (DATK-32)), TCR gamma/delta Monoclonal Antibody (eBioGL3 (GL-3, GL3)), PE (eBioscience,12-5711-82,clone eBioGL3 (GL-3, GL3)), CD8b Monoclonal Antibody (eBioH35-17.2 (H35-17.2)), PE-Cyanine7 (eBioscience,25-0083-82,clone eBioH35-17.2 (H35-17.2)), CD3e Monoclonal Antibody (145-2C11), PE (eBioscience,12-0031-82,clone 145-2C11), CD3e Monoclonal Antibody (145-2C11), eFluor 450 (eBioscience,48-0031-82,clone 145-2C11), FOXP3 Monoclonal Antibody (FJK-16s), APC (eBioscience,17-5773-82,clone FJK-16s), CD25 Monoclonal Antibody (PC61.5), PE-Cyanine7 (eBioscience,25-0251-81,clone PC61.5), CD25 Monoclonal Antibody (PC61.5), Alexa Fluor 488 (eBioscience,53-0251-82,clone PC61.5), CD19 Monoclonal Antibody (eBio1D3 (1D3)), PE-Cyanine7 (eBioscience,25-0193-81,clone eBio1D3 (1D3)), CD11b Monoclonal Antibody (M1/70), PE (eBioscience,12-0112-82,clone M1/70), CD27 Monoclonal Antibody (LG.7F9), FITC (eBioscience,11-0271-82,clone LG.7F9), CD122 Monoclonal Antibody (TM-b1 (TM-beta1)), PE (eBioscience,12-1222-81,clone TM-b1 (TM-beta1)), CD127 Monoclonal Antibody (A7R34), FITC (eBioscience,11-1271-82,clone A7R34), KLRG1 Monoclonal Antibody (2F1), eFluor 450 (eBioscience,48-5893-82,clone 2F1), EOMES Monoclonal Antibody (Dan11mag), Alexa Fluor 488 (eBioscience,53-4875-80,clone Dan11mag), T-bet Monoclonal Antibody (eBio4B10 (4B10)), PE (eBioscience,12-5825-80,clone eBio4B10 (4B10)), Ki-67 Monoclonal Antibody (SolA15), eFluor 450 (eBioscience,48-5698-80,clone SolA15), CD335 (NKp46) Monoclonal Antibody (29A1.4), PE (eBioscience,12-3351-80,clone 29A1.4), FITC anti-mouse Ly-6G/Ly-6C (Gr-1) Antibody (eBioscience,108406,clone RB6-8C5), CTLA-4 Monoclonal Antibody (1B8), FITC (ThermoFisher,HMCD15201,clone 1B8), CD45 Monoclonal Antibody (HI30), eFluor 450 (eBioscience,48-0459-41,clone HI30), CD56 (NCAM) Monoclonal Antibody (TULY56), APC (eBioscience,17-0566-41,clone TULY56), CD16 Monoclonal Antibody (B73.1), PE (eBioscience,12-0167-42,clone B73.1), CD3 Monoclonal Antibody (OKT3), eFluor 450 (eBioscience,48-0037-42,clone OKT3), CD8a Monoclonal Antibody (RPA-T8), PE-Cyanine7 (eBioscience,25-0088-42,clone RPA-T8), CD335 (NKp46) Monoclonal Antibody (9E2), PE-Cyanine7 (eBioscience,25-3359-41,clone 9E2), KLRG1 Monoclonal Antibody (13F12F2), Alexa Fluor 488 (eBioscience,53-9488-41clone 13F12F2), CD122 Monoclonal Antibody (TU27), FITC (eBioscience,11-1228-41,clone TU27), CD132 Monoclonal Antibody (TUGh4), PE (eBioscience,12-1329-42 ,clone TUGh4), CD107a (LAMP-1) Monoclonal Antibody (eBioH4A3), eFluor 660 (eBioscience,50-1079-41,clone eBioH4A3);
Antibodies used for Immunostaining and Western Blotting include: Anti-Ki67 antibody (ab15580) (Abcam ab15580,Polyclonal), Anti-CD31 antibody (ab28364) (Abcam,ab28364,Polyclonal), Cleaved Caspase-3 (Asp175) Antibody #9661 (CST,9661S,Polyclonal), Granzyme B Antibody #4275 (CST,4275S,Polyclonal), Perforin Antibody (Mouse Specific) #3693 (CST,3693S,Polyclonal), Phospho-Akt (Ser473) (D9E) XP¨

Nature Medicine: doi:10.1038/nm.4496

10. Eukaryotic cell lines

a. State the source of each eukaryotic cell line used.

HEK293 and HCT-116 cells were purchased from ATCC. YUMM1.7 was provided by Marcus Bosenberg and reported previously (6). MC38 was purchased from Kerafast (Boston, MA). Cells were all tested for mycoplasma and they were negative.

b. Describe the method of cell line authentication used.

The cell lines were validated by the commercial vendors.

c. Report whether the cell lines were tested for mycoplasma contamination.

Cells have been routinely tested for mycoplasma and they were negative.

d. If any of the cell lines used are listed in the database of commonly misidentified cell lines maintained by ICLAC, provide a scientific rationale for their use.

No

Animals and human research participants

Policy information about studies involving animals; when reporting animal research, follow the ARRIVE guidelines

11. Description of research animals

Provide all relevant details on animals and/or animal-derived materials used in the study.

Dkk2-/- mice were described previously (1,2) and have been backcrossed to C57Bl background for more than 7 generation. Ncr1-Cre mice were also described previously (3). NSG (NOD.Cg-PrkdcscidIl2rgtm1Wjl/SzJ), ApcMin/+ (C57BL/6J-ApcMin/J) and MX1Cre [B6.Cg-Tg(Mx1-cre)1Cgn/J] mice were acquired from the Jackson Laboratory. Wildtype C57BL/6 mice were purchased from Envigo (Harlan). The LoxP-floxed Lrp5 (Lrp5f/f) and Lrp6 (Lrp6f/f) mice were obtain from Bart Williams. The Lrp5f/f and Lrp6f/f mice were backcrossed to C57/BL6 for more than 7 generations before being intercrossed with MX1Cre. LRP5 and LRP6 gene disruption was induced by intraperitoneal injection of the Lrp5fl/flMX1Cre mice with 40 µl poly-I:C (10 mg/mL) every other day for 4 treatments. The mice were used for NK cell isolation three weeks after the poly-I:C treatment. For adoptive bone marrow transfer, bone marrows from the Lrp5fl/flMX1Cre mice were transferred to lethally irradiated C57/BL6 mice (8 weeks old female) via retro-orbital injection. After recovery (8 weeks), the mice were treated with poly-I:C and used in experiments three weeks after poly-I:C treatment. Age and sex of the mice used in the study are described in the manuscript. Mice were cared for in accordance with US National Institutes of Health guidelines, and all procedures were approved by the Yale University Animal Care and Use Committee.

Policy information about studies involving human research participants

12. Description of human research participants

Describe the covariate-relevant population characteristics of the human research participants.

No human research participants are involved in the current study.

Nature Medicine: doi:10.1038/nm.4496

nature research

Corresponding author(s): Dianqing Wu

Flow Cytometry Reporting Summary

Form fields will expand as needed. Please do not leave fields blank.

Data presentation

For all flow cytometry data, confirm that:

☒ 1. The axis labels state the marker and fluorochrome used (e.g. CD4-FITC).

☒ 2. The axis scales are clearly visible. Include numbers along axes only for bottom left plot of group (a 'group' is an analysis of identical markers).

☒ 3. All plots are contour plots with outliers or pseudocolor plots.

☒ 4. A numerical value for number of cells or percentage (with statistics) is provided.

Methodological details

5. Describe the sample preparation.

Preparation of tumor infiltrating leukocytes. Tumors were minced using scissors and scalpel blades and incubated with a digestion buffer [RPMI1640, 5% FBS, 1% PS, 25mM HEPES and 300U collagenase (Sigma C0130)] in a shaker for 2h at 37°C. Disperse cells were filtered through a 70 µm cell strainer to eliminate clumps and debris. After centrifugation for 5 minutes (500xg) at 4°C, cell pellets were resuspended in the Red Blood Cell Lysis Buffer (Sigma R7757) and incubated at RT for 5 min to remove erythrocytes. Cells were pelleted again, resuspended and incubated in 0.05% Trypsin/EDTA at 37°C for 5min, followed by DNA digestion with the addition of Type I DNase (1 µg/ml final, Sigma D4263) for 5 min. Trypsin digestion was stopped by the addition of FBS to 5%, and cells were filtered again by a 40 µm cell strainer. Finally, the cells were pelleted again and resuspended in PBS at a concentration of 2 X 107.

Cells in single cell suspension were fixed with 2% PFA (Santa-Cruz sc-281692). After washing with a Flow Cytometry Staining Buffer (eBioscience 00-4222-26), cells were stained with antibodies for cell surface markers for 1 hour on ice in the dark. For staining of intracellular proteins, the cells were washed and resuspended in the Permeabilization Buffer (BD 554723) and stained by antibodies in the Permeabilization Buffer for 1 hour on ice in the dark. The cells were then pelleted and resuspended in the Flow Cytometry Staining Buffer for flow cytometry analysis.

Preparation and treatment of mouse primary NK, CD8+ and IEL cells. Mouse primary NK and CD8+ T cells were isolated from the spleens of female mice (8 weeks old) by using the NK cell and CD8+ T cell isolation kits according to the manufacturer's instructions (Miltenyi Biotec #130-090-864 and #130-104-075), respectively. Primary NK cells were cultured in RPMI-1640 (Gibco, 11875-093) supplemented with 10% FBS, penicillin (100 U/ml), streptomycin (100 µg/ml), 2-mercaptoethanol (500µM) and HEPES (10mM) at 37 °C supplemented with 5% CO2 in the presence of recombinant murine IL-15 (50 ng/ml) for 24 hours before treatment with DKK2, CHIR99021, or WNT3A. CD8+ T cells were cultured in the same culture medium and condition as NK cells, but supplemented with IL-15 (200 ng/ml) and IL-15 Rα (1 µg/ml recombinant Mouse IL-15 receptor alpha Fc chimera Protein from R&D) for 96 hours before DKK2 treatment.

Mouse primary intraepithelial lymphocytes (IELs) were prepared as described in 8,9. In brief, the small intestine was everted, divided into four pieces, and washed twice in phosphate-buffered saline (PBS) containing 100 U/ml penicillin/ streptomycin. The specimens were then incubated with stirring at 37°C in prewarmed Ca2+ and Mg2+-free Hanks' solution containing 100 U/ml penicillin-streptomycin, 5% fetal calf serum (FCS), 2 mM dithiothreitol (DTT), and 5mM EDTA for 30 min, followed by vigorous shaking for 30s. The supernatants were passed over two nylon wool columns to remove undigested tissue debris. The lymphocytes obtained were pooled and enriched on a discontinuous (40% and 70%) Percoll density gradient. Cells at the interface between the 40% and 70% fractions (IELs)

Nature Medicine: doi:10.1038/nm.4496

	were collected for treatment with IL-15 (200 ng/ml) and DKK2 (400 ng/ml), followed by flow analysis. Preparation of human NK cells. Peripheral blood mononuclear cells from normal humans were purchased from ZenBio (SER-PBMC-200). Human NK cells were isolated from the PBMCs by using the human NK cell isolation kit according to the manufacturer's instruction (Miltenyi Biotec # 130-092-657). Human NK cells were cultured in RPMI-1640 (Gibco, 11875-093) supplemented with 10% heat-inactivated FBS, penicillin (100 U/ml), streptomycin (100 µg/ml), 2-mercaptoethanol (500µM) and HEPES (10mM) at 37 °C supplemented with 5% CO2 in the presence of recombinant human IL-15 (50 ng/ml) before treatment with recombinant human DKK2 protein.
6. Identify the instrument used for data collection.	BD LSRII flow cytometer
7. Describe the software used to collect and analyze the flow cytometry data.	Flowjo v10
8. Describe the abundance of the relevant cell populations within post-sort fractions.	N/A
9. Describe the gating strategy used.	Gating strategies are clearly described in the figure legends. Basically, Live cells were gated with FCS and SSC and subsequently for CD45. cells are gated with various markers as indicated in the figures

Tick this box to confirm that a figure exemplifying the gating strategy is provided in the Supplementary Information. ☐

Nature Medicine: doi:10.1038/nm.4496